iScience

CellPress
OPEN ACCESS

Article

Ventral pallidal glutamatergic neurons regulate wakefulness and emotion through separated projections

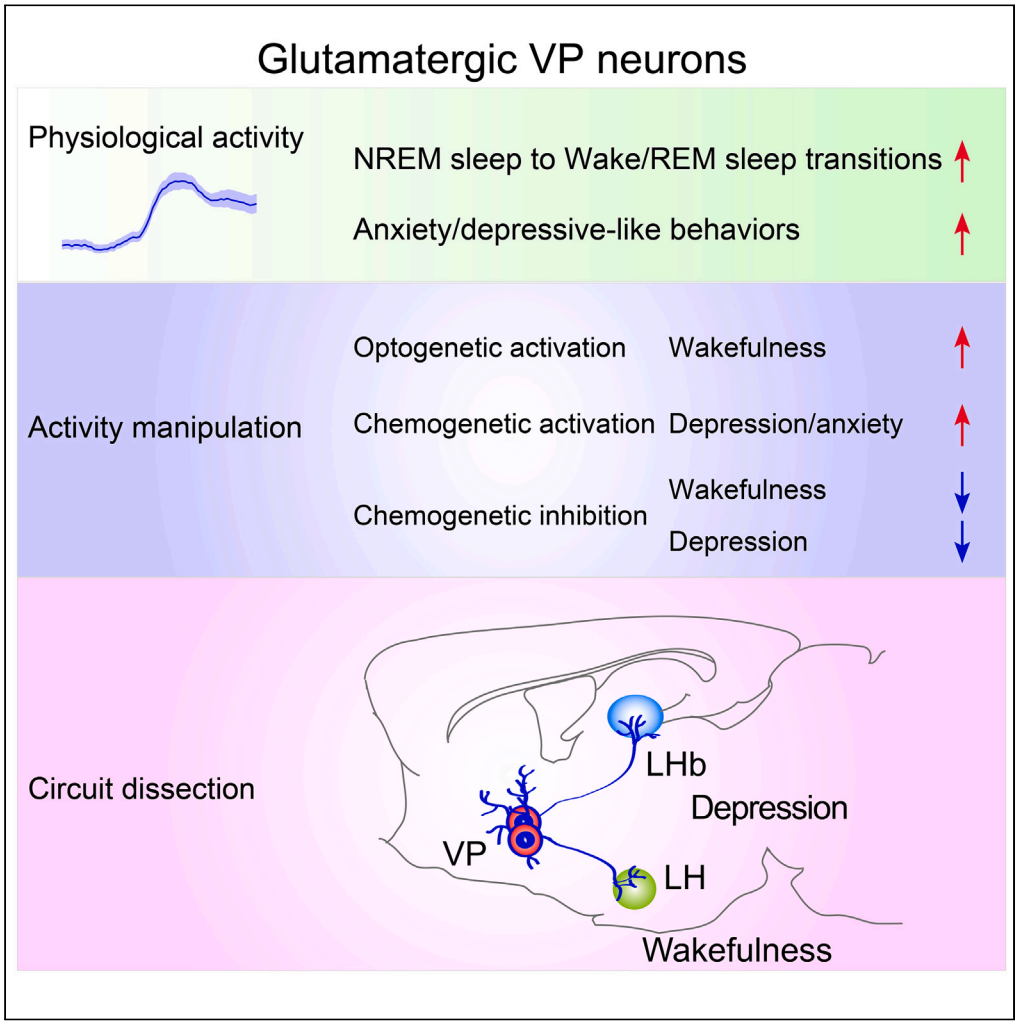

Yan-Jia Luo, Jing Ge, Ze-Ka Chen, ..., Wei-Min Qu, Zhi-Li Huang, Ya-Dong Li

quweimin@fudan.edu.cn (W.-M.Q.)
huangzl@fudan.edu.cn (Z.-L.H.)
yadlee@126.com (Y.-D.L.)

Highlights

The activity of VP^{Vglut2} neurons is associated with states of wakefulness and emotion

VP^{Vglut2} neurons dual regulation of wakefulness and anxiety/depressive-like behaviors

VP^{Vglut2} neurons regulate wakefulness and emotion through LH and LHb, respectively

Luo et al., iScience 26, 107385
August 18, 2023
https://doi.org/10.1016/j.isci.2023.107385

iScience

CellPress
OPEN ACCESS

Article

Ventral pallidal glutamatergic neurons regulate wakefulness and emotion through separated projections

Yan-Jia Luo,[1,2] Jing Ge,[1] Ze-Ka Chen,[1] Zi-Long Liu,[1] Michael Lazarus,[3] Wei-Min Qu,[1,*] Zhi-Li Huang,[1,4,*] and Ya-Dong Li[1,5,6,*]

SUMMARY

Insomnia is often comorbid with depression, but the underlying neuronal circuit mechanism remains elusive. Recently, we reported that GABAergic ventral pallidum (VP) neurons control wakefulness associated with motivation. However, whether and how other subtypes of VP neurons regulate arousal and emotion are largely unknown. Here, we report glutamatergic VP (VP^{Vglut2}) neurons control wakefulness and depressive-like behaviors. Physiologically, the calcium activity of VP^{Vglut2} neurons was increased during both NREM sleep-to-wake transitions and depressive/anxiety-like behaviors in mice. Functionally, activation of VP^{Vglut2} neurons was sufficient to increase wakefulness and induce anxiety/depressive-like behaviors, whereas inhibition attenuated both. Dissection of the circuit revealed that separated projections of VP^{Vglut2} neurons to the lateral hypothalamus and lateral habenula promote arousal and depressive-like behaviors, respectively. Our results demonstrate a subtype of VP neurons is responsible for wakefulness and emotion through separated projections, and may provide new lines for the intervention of insomnia and depression in patients.

INTRODUCTION

Sleep disorders are often associated with mental diseases such as depression and anxiety. For example, up to 80% of individuals with major depressive disorder (MDD) also experience insomnia symptoms.[1–3] However, the underlying neuronal circuits that control insomnia and depressive-like behaviors in healthy and diseased brains are not fully understood. Wake-promoting brain regions are well known to regulate memory,[4] food intake,[5,6] reward,[6] and motivation,[7,8] but also regulate anxiety/depressive-like behaviors. Functional dissection of neuronal circuits that control aberrant arousal associated with depressive- and anxiety-like behaviors may help us understand how mental disorders occur and provide new approaches for treating mental diseases and sleep disorders.

In the clinic, depression is more difficult to treat in the presence of insomnia, but the treatment of depression may improve symptoms of insomnia in patients with mild to moderate depression.[9] In addition, the risk of depression recurrence is increased when insomnia persists after treatment of depression alone.[10] This clinical phenomenon suggests that shared neurons or neuronal circuits may regulate depression and associated insomnia. The ventral basal ganglia limbic system plays a key role in regulating anxiety and depressive-like behaviors. As a major component of the ventral basal ganglia, substantial studies have demonstrated that the ventral pallidum (VP) is capable of integrating and transmitting motivation,[11] reward,[12–14] as well as stress,[15] and depression-related[16,17] signals in the brain. A recent study found that orexin prevents depressive-like behavior by exciting GABAergic VP neurons,[18] while, parvalbumin (PV)-positive neurons in the VP projecting to either the lateral habenula (LHb) or ventral tegmental area (VTA) contributed to depression.[16] These findings suggest that VP can integrate multi-inputs and transmit outputs in regulating depression.

Interestingly, the VP also plays a dominant role in controlling wakefulness. Anatomically, the most dominant input to VP is the nucleus accumbens (NAc), where dopamine D_2R positive GABAergic neurons promote sleep with less motivation by inhibiting VP,[19] suggesting that VP is a wake-promoting region. Indeed, our recent findings have shown that VP GABAergic neurons are essential for heightened arousal related to motivation.[7] Functionally, the VP plays a critical role in the processing and execution of motivated

[1]Department of Pharmacology, School of Basic Medical Sciences, State Key Laboratory of Medical Neurobiology and MOE Frontiers Center for Brain Science, and Institutes of Brain Science, Fudan University, Shanghai 200032, China

[2]Department of Anesthesiology, Shanghai Ninth People's Hospital, Shanghai Jiao Tong University School of Medicine, Shanghai 200011, China

[3]International Institute for Integrative Sleep Medicine (WPI-IIIS) and Institute of Medicine, University of Tsukuba, 1-1-1 Tennodai, Tsukuba, Ibaraki 305-8575, Japan

[4]Department of Anesthesiology, Zhongshan Hospital, Fudan University, Shanghai 200032, China

[5]Songjiang Research Institute, Shanghai Songjiang District Central Hospital, Shanghai Jiao Tong University School of Medicine, Shanghai 201699, China

[6]Lead contact

*Correspondence: quweimin@fudan.edu.cn (W.-M.Q.), huangzl@fudan.edu.cn (Z.-L.H.), yadlee@126.com (Y.-D.L.)

https://doi.org/10.1016/j.isci.2023.107385

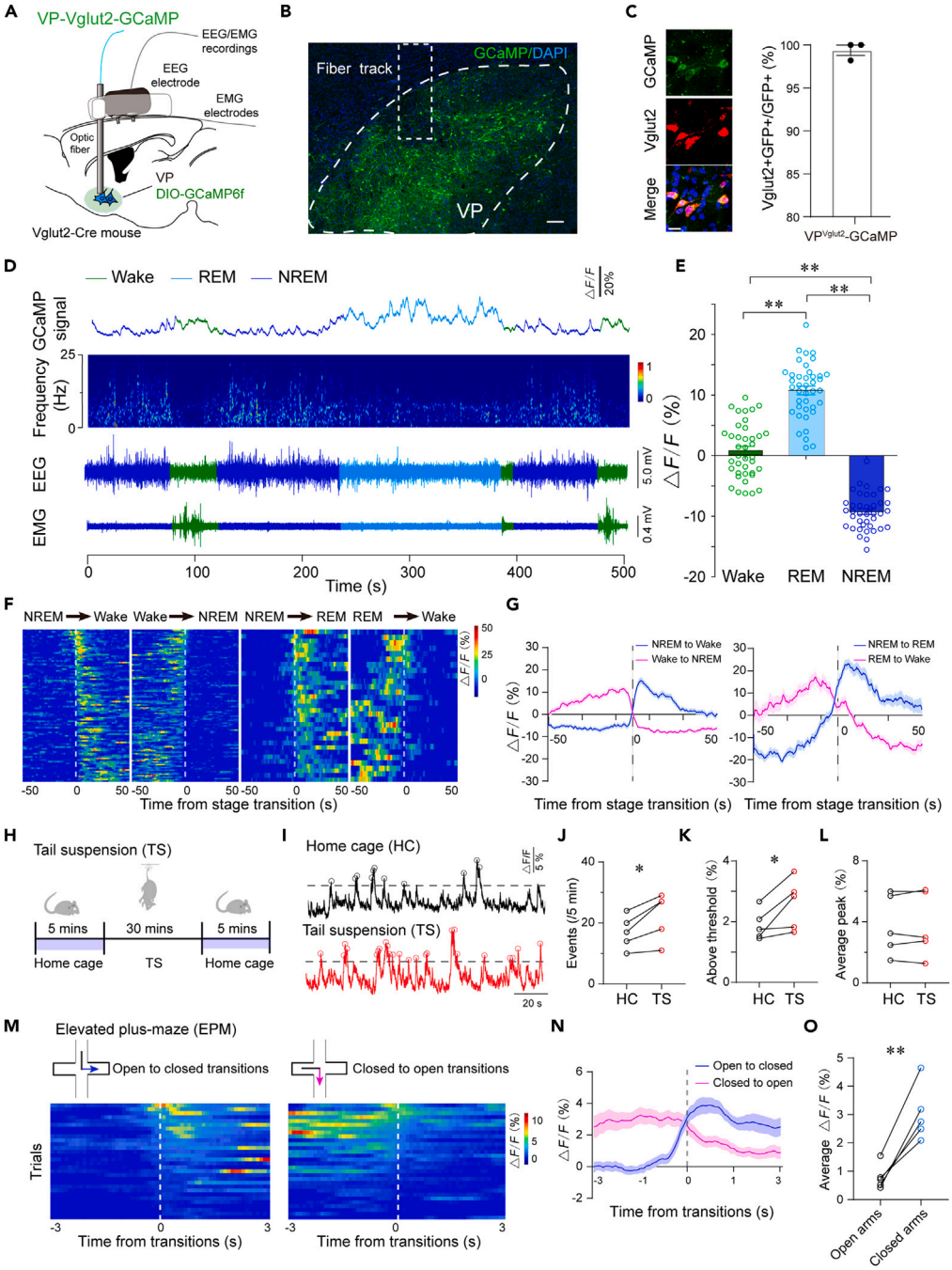

Figure 1. Dynamic activity of VP^{Vglut2} neurons across sleep-wake stages and emotional changes

(A) Schematic of *in vivo* fiber-photometry recordings of calcium activity of VP^{Vglut2} neurons and EEG/EMGs.

(B) Image showing expression of GCaMP6f in the lateral VP. Dashed box indicates the track of the fiber cannula. Scale bar = 200 μm.

(C) GCaMP6f-expressing cells were also *Vglut2* mRNA positive, and quantification of GCaMP6f positive cells (GFP+) double staining for Vglut2 mRNA in the VP. Scale bar = 20 μm. n = 3 mice.

(D) Representative fluorescent traces, heatmap of relative EEG power, and EEG/EMG traces across spontaneous sleep-wake states. The lowest calcium activity was in the NREM sleep, with high EEG delta power and quiet EMG. Calcium activity was higher in wakefulness. The highest calcium activity was in REM sleep.

(E) ΔF/F peaks during wakefulness, NREM sleep, and REM sleep. n = 4 mice, 10 sessions per mouse, **p < 0.01, one-way ANOVA followed by Tukey's *post hoc* test.

Figure 1. *Continued*

(F) Fluorescent signals aligned to arousal state transitions. Upper panel: Individual transitions with color-coded fluorescent intensities (NREM–wake, n = 94; wake–NREM, n = 111; NREM–REM, n = 33; REM–wake, n = 29).

(G) Average calcium transients from all the transitions were expressed as the mean ± SEM. The mean ΔF/F was increased in NREM sleep-to-wake or REM sleep transitions but decreased in wake-to-NREM or REM-to-wake transitions.

(H) Diagram of TS combing calcium recording.

(I–L) Sample traces (I), events (J), above threshold (%) (K), and average peak (%) (L) of calcium activity of VP^{Vglut2} neurons before and after tail suspension. n = 5 mice, *p < 0.05, paired *t*-test.

(M) Heatmap of calcium activity of VP^{Vglut2} neurons in the EPM test. Time '0' indicates transitions from closed-open arms or open-closed arms (30 trials from 5 mice).

(N) Average calcium activity of VP^{Vglut2} neurons in EPM test in closed-to-open arms or open-to-closed arms transitions.

(O) Average ΔF/F in closed and open arms from (N). n = 5 mice, **p < 0.01, paired *t*-test.

behaviors and mental health (e.g., addiction, depression).[20] The VP is a highly heterogeneous structure consisting of GABAergic, glutamatergic, and a small number of cholinergic neurons.[20] Whether and how glutamatergic and cholinergic VP neurons regulate arousal related to emotion remains poorly understood. Given that VP-regulated behaviors are associated with increased arousal (e.g., motivation[21]) or accompanied by insomnia (e.g., depression[22]), we hypothesized that a subpopulation of VP neurons plays a role in regulating wakefulness related to emotion.

In this study, we aimed to uncover the role of glutamatergic VP (VP^{Vglut2}) neurons and cholinergic VP (VP^{ChAT}) neurons in regulating arousal and emotion in mice. Using *in vivo* fiber photometry combined with polysomnographic methods, we found that VP^{Vglut2} neurons are active in non-rapid eye movement (NREM) sleep-wake/REM sleep transitions and anxiety/depressive-like behaviors. Chemogenetic and optogenetic manipulations revealed the causal role of VP^{Vglut2} neurons in increasing wakefulness and depressive-like behaviors. Importantly, we found that distinct circuit pathways from the VP^{Vglut2} neurons regulate wakefulness and depressive-like behaviors. Our results suggest that VP^{Vglut2} neurons are a potential target for treating patients with co-morbid depression and insomnia.

RESULTS

Increased population activity of VP^{Vglut2} neurons in the wakefulness

To investigate whether the activities of VP^{Vglut2} neurons are physiologically associated with spontaneous sleep-wake cycles in mice, we recorded the calcium activity of these neurons using *in vivo* fiber photometry.[8] The AAV-hSyn-DIO-GCaMP6f construct was injected unilaterally into the VP of Vglut2-Cre mice, and an optical fiber was implanted into the VP. Calcium activity and electroencephalograms (EEGs)/electromyograms (EMGs) were recorded simultaneously in freely moving mice within their home cages (Figure 1A). GFP fluorescence showed that GCaMP6f-expressing cells were located in the dorsolateral VP (Figure 1B). Fluorescence *in situ* hybridization confirmed that nearly 99.4% GFP+ neurons were *Vglut2* positive (Figure 1C), indicating that GCaMP was correctly expressed in VP^{Vglut2} neurons. Interestingly, we observed that changes in the population activity of VP^{Vglut2} neurons were consistently associated with sleep-wake-stage transitions (Figure 1D). Specifically, VP^{Vglut2} neurons displayed the lowest calcium activity during non-rapid eye movement (non-REM, NREM) sleep and had moderate activity in wakefulness (Figure 1E). The population activity of VP^{Vglut2} neurons was significantly higher during REM sleep, compared to other sleep-wake stages (Figure 1E), indicating the activity of these neurons may be also associated with REM sleep or related functions. Importantly, VP^{Vglut2} neurons showed a significant decrease in calcium activity (~20%) at wake-to-NREM sleep transitions, with a similar level of increase at NREM sleep-to-wake transitions (Figures 1F and 1G), suggesting that VP^{Vglut2} neurons are wake-and REM sleep-active neurons. These results show that VP^{Vglut2} neurons are silent during NREM sleep, active during wakefulness, and highly active during REM sleep.

Dynamic activities of VP^{Vglut2} neurons in anxiety and depressive-like behaviors

Having clarified the increased calcium activity of VP^{Vglut2} neurons during sleep-wake transitions, we decided to investigate the physiological activity of VP^{Vglut2} neurons in regulating anxiety or depressive-like behaviors. Similar to monitoring the activity of VP^{Vglut2} neurons in EEG recording, we used the same fiber photometry system to record calcium activity of VP^{Vglut2} neurons during two emotional behavioral tasks, elevated plus-maze (EPM) and tail suspension (TS), to assess anxiety and depressive-like behaviors, respectively. In the TS test, calcium activity was first recorded for 5 min in the home cage before TS as a baseline (see, 'HC'). Then, mice were subjected to TS for 30 min to induce depressive-like state.

Immediately after that, calcium activity was recorded for the same mice for an additional 5 min (see, 'TS', Figures 1H and 1I). We analyzed events, above thresholds and the average peak of calcium activity, based on our established method.[4,23] Notably, TS significantly increased the event and time above thresholds of calcium activity of VP^{Vglut2} neurons, but not the average peak (Figures 1I–1L). These results suggest that VP^{Vglut2} neurons are active in depressive-like behaviors.

To further monitor the dynamic activity of VP^{Vglut2} neurons during emotional changes, we recorded the calcium activity of VP^{Vglut2} neurons in the EPM assay. The calcium activity of VP^{Vglut2} neurons was analyzed 3 s before and after transitions from open to closed arm (open to closed transitions) or closed to open arm (closed to open transitions). Calcium activity was visualized as a heatmap (Figure 1M). Impressively, the calcium activity of VP^{Vglut2} neurons was increased dramatically during open to closed transitions but decreased during closed to open transitions (Figures 1M and 1N). Meanwhile, the average $\Delta F/F$ was also increased in the closed arms (Figure 1O). Since mice residing in closed arms reflect an anxious state and calcium activity of VP^{Vglut2} neurons was increased in the closed arms, these results suggest increased activity of VP^{Vglut2} neurons in anxiety-like behavior. Overall, these results suggest that the activity of VP^{Vglut2} neurons may be physiologically involved in the regulation of wakefulness and associated anxiety/depressive-like behaviors.

Optogenetic activation of VP^{Vglut2} neurons increased wakefulness

To explore the causal role of the activity of VP^{Vglut2} neurons and wakefulness, we decided to use optogenetics to activate VP^{Vglut2} neurons specifically. The AAV-hSyn-DIO-ChR2-mCherry construct or AAV-hSyn-DIO-mCherry control virus was injected bilaterally into the VP of Vglut2-Cre mice with implantation of optic fibers above the VP (Figure 2A). Blue laser at 473 nm was administered during simultaneous EEG/EMG recordings. *In vitro* electrophysiological recording verified that optogenetic stimulation at 30 Hz could elicit action potentials in a VP^{Vglut2} neuron with 100% fidelity (Figure 2B). Immunohistochemical labeling confirmed that optogenetic stimulation dramatically increased c-Fos expression in mCherry+ neurons in the VP (Figure 2C). These data demonstrate that optogenetic stimulation at 30 Hz induced robust activation of VP^{Vglut2} neurons. It is worth noting that we used a relatively high frequency because the firing frequency of VP^{Vglut2} neurons ranges from 15 to 20 Hz at baseline and reaches 30–40 Hz in the events in *in vivo* electrophysiological recording.[11] Importantly, *in vivo* optogenetic activation of VP^{Vglut2} neurons induced immediate transitions from NREM sleep to wakefulness (Figure 2D). Optogenetic stimulation was given for 16 s in a trial, and the arousal can last for nearly 30 s. We also analyzed the EEG power density and power spectrum during optogenetic stimulation. The EEG power density decreased in the 1.5–3 Hz and 5–6 Hz bands, as mice spent more time in wakefulness (Figure 2E). The EEG power spectrum was slightly decreased, with no statistical difference (Figure 2F). These data indicate that optogenetic activation of VP^{Vglut2} neurons promotes behavioral arousal.

We then decided to test whether long-term stimulation of VP^{Vglut2} neurons could maintain wakefulness during the light phase. Time course analysis showed that optogenetic stimulation of VP^{Vglut2} neurons (10 s ON/20 s OFF, 5 ms duration, 120 cycles) for 1 h increased wakefulness in the first 30 min (Figure 2G). The total amount of wakefulness was increased by 72.56% in ChR2-mice compared with the baseline during 1 h optogenetic stimulation (Figure 2H). Notably, optogenetic activation increased the possibility of NREM sleep to wake transitions only in the frequency >20 Hz (Figure 2I). These results suggest that optogenetic activation of VP^{Vglut2} neurons induced wakefulness that was not of long duration. This is in sharp contrast to the optogenetic activation of glutamatergic basal forebrain (BF) neurons at 10 Hz which fully blocked NREM sleep for 1 h,[24] indicating glutamatergic VP neurons play a different role to BF neurons in regulating wakefulness. Taken together, optogenetic stimulation of VP^{Vglut2} neurons induced wakefulness from NREM sleep, indicating that aberrant activation of VP glutamatergic neurons may cause insomnia.

Chemogenetic inhibition of VP^{Vglut2} neurons slightly decreased wakefulness

Next, in order to investigate whether the activity of VP^{Vglut2} neurons is required for wakefulness, we used chemogenetics to inhibit VP^{Vglut2} neurons. The AAV-hSyn-DIO-hM4Di-mCherry construct was injected bilaterally into the VP of Vglut2-Cre mice (Figure 3A). Immunohistochemical labeling confirmed that mCherry was accurately expressed in the VP, and CNO injection decreased c-Fos expression in mCherry+ neurons from 31.4% to 7.8% (Figures 3B and 3C), indicating inhibition of VP^{Vglut2} neurons. Chemogenetic inhibition of VP^{Vglut2} neurons only slightly decreased wake time for 2 h after CNO injection from 86.51 min to 66.51 min, concurrently, it increased NREM sleep from 30.75 min to 52.14 min, but did not significantly

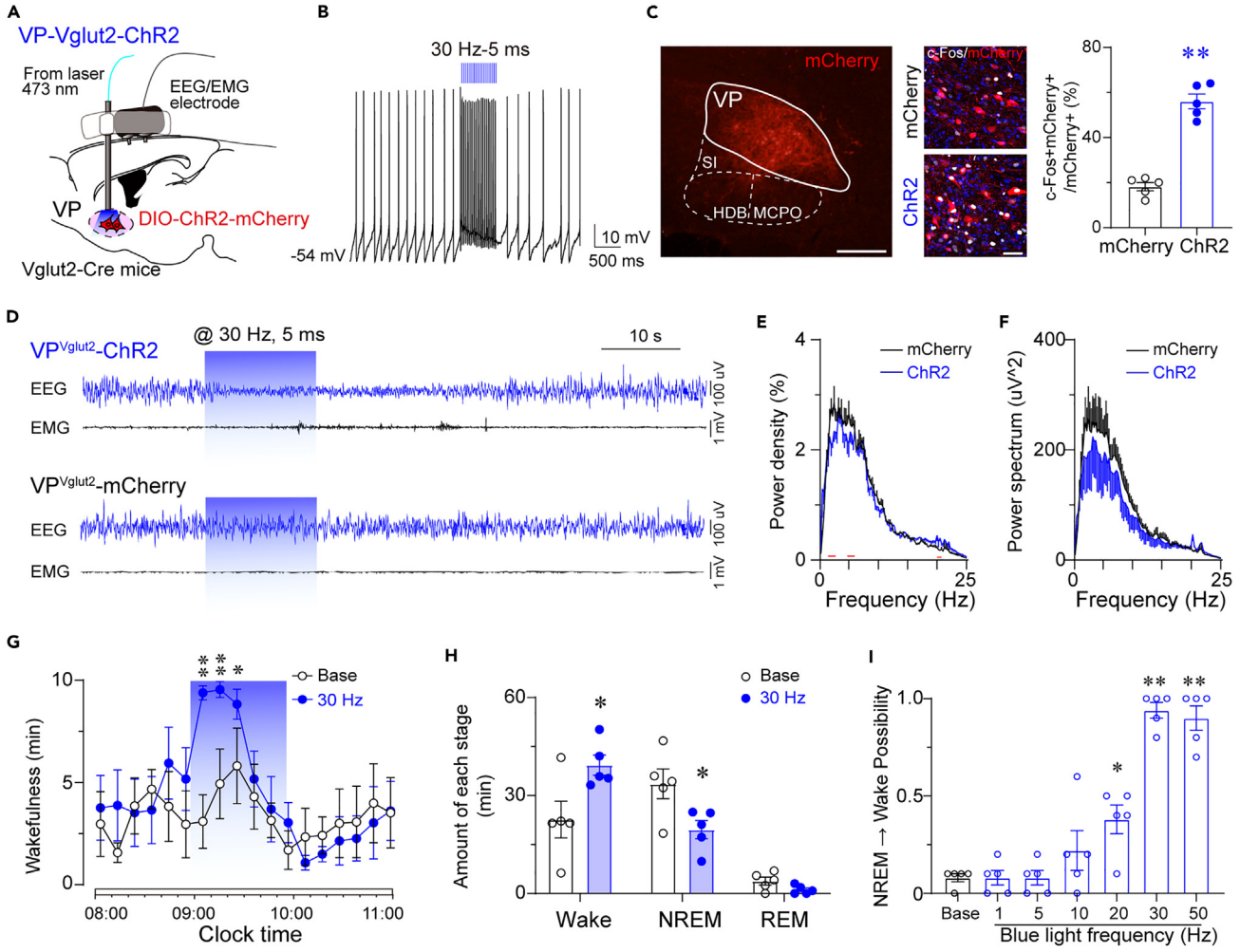

Figure 2. Optogenetic activation of VP^{Vglut2} neurons induces wakefulness

(A) Sagittal diagram for *in vivo* optogenetic stimulation of VP glutamatergic neurons in Vglut2-Cre mice.

(B) Optogenetic stimulation at 30 Hz induced action potentials in a ChR2-mCherry positive glutamatergic neuron.

(C) Optogenetic stimulation increased c-Fos expression in mCherry+ neurons in the VP. Left, Representative image of ChR2-mCherry expression in the VP. Scale bar = 200 μm. Double staining of mCherry and c-Fos confirmed that abundant c-Fos immunoreactivity in ChR2-mCherry neurons following optogenetic stimulation of VP. Scale bar = 50 μm. Right, Quantification of c-Fos+mCherry+ cells divided by the total number of mCherry+ cells in the VP following optogenetic stimulation in mCherry or ChR2-mCherry mice. *$p < 0.05$, unpaired *t*-test (n = 5 mice per group). MCPO, magnocellular preoptic nucleus; HDB, nucleus of the horizontal limb of the diagonal band; SI, substantia innominate.

(D) Representative EEG/EMG traces show that acute optogenetic stimulation (30 Hz/5 ms) applied during NREM sleep induced a transition to wake in a ChR2-mCherry mouse (upper), but not an mCherry mouse (below).

(E) EEG power density during optogenetic stimulation in VP^{Vglut2}-ChR2 or VP^{Vglut2}-mCherry mice. Red lines indicate statistical differences (n = 5 mice per group; $p < 0.05$).

(F) EEG power spectrum during optogenetic stimulation in VP^{Vglut2}-ChR2 or VP^{Vglut2}-mCherry mice. n = 5 mice per group.

(G) Time course of wakefulness before, during, and after 1-h optogenetic activation of VP glutamatergic neurons.

(H) Amount of wakefulness, NREM sleep, and REM sleep during 1-h optogenetic stimulation of VP glutamatergic neurons, compared to baseline. n = 5 mice, *$p < 0.05$, paired *t*-test.

(I) Possibility of transitions from NREM sleep to wakefulness after optogenetic stimulation at different frequencies. n = 5 mice, *$p < 0.05$, **$p < 0.01$ using repeated-measures ANOVA, followed by Tukey *post hoc* test.

change the amount of REM sleep (Figures 3D and 3E). Interestingly, the EEG power spectrum was also slightly increased in low frequency (2–8 Hz), probably due to the increased amount of NREM sleep (Figures 3F and 3G). These data suggest that decreasing activity of VP^{Vglut2} neurons induces a lower amount of wakefulness. Combining chronic optogenetic activation of VP^{Vglut2} neurons, which increases wakefulness, and chemogenetic inhibition, which decreases wakefulness, with acute optogenetic

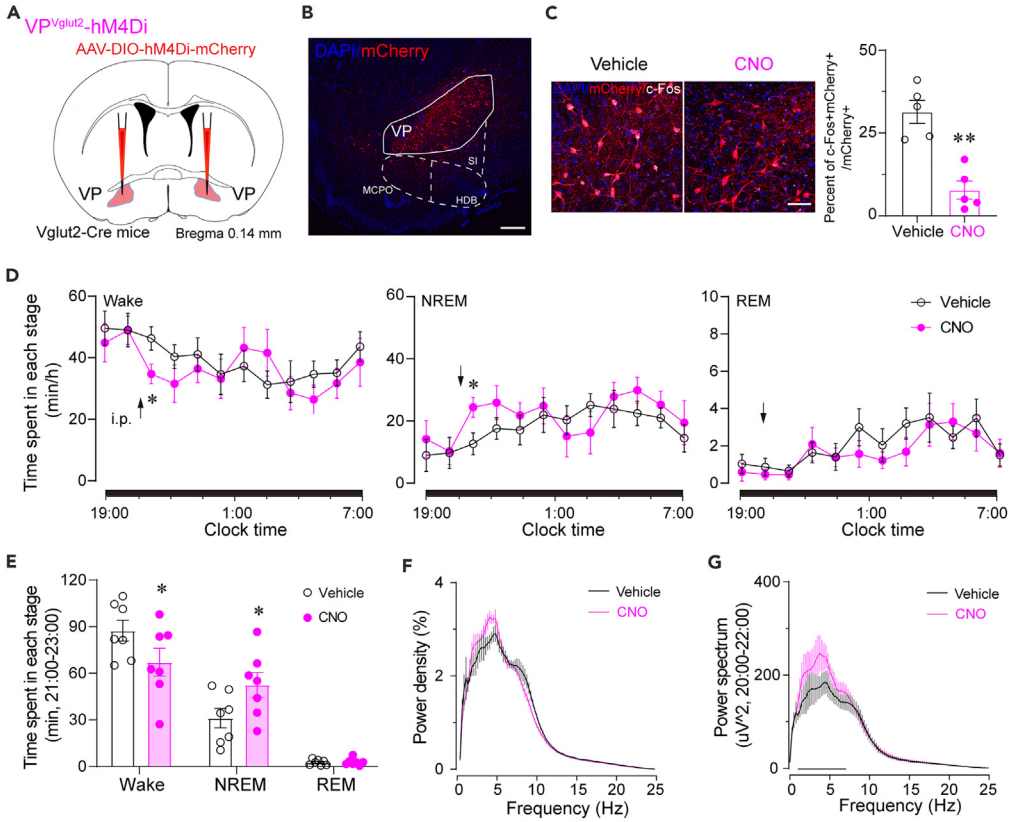

Figure 3. Chemogenetic inhibition of VP^{Vglut2} neurons slightly decreases wakefulness

(A) Schematic diagram of chemogenetic inhibition of VP^{Vglut2} neurons.

(B) The expression of hM4Di-mCherry in the VP. Scale bar = 100 μm.

(C) Left: c-Fos expression in mCherry+ neurons after vehicle or CNO injection. Scale bar = 50 μm. Right: Quantification of c-Fos+mCherry+ cells divided by the total number of mCherry+ cells in the VP after vehicle or CNO injection. n = 5 mice per group. **p < 0.01, unpaired *t*-test.

(D) Time course changes in wakefulness, NREM sleep, and REM sleep after administration of vehicle or CNO. n = 7 mice. *p < 0.05, repeated-measures ANOVA followed by paired *t*-test.

(E) Total time spent in Wake, NREM, and REM sleep from 21:00-23:00 after administration of vehicle or CNO. n = 7 mice. *p < 0.05, paired *t*-test.

(F and G) EEG power density (F) and power spectrum (G) from 21:00-23:00 after administration of vehicle or CNO. n = 7 mice; * or black line indicates p < 0.05 by paired *t*-test.

activation induced immediately NREM sleep-wake transitions, we conclude that activation of VP^{Vglut2} neurons induces wakefulness.

VP^{ChAT} neurons did not regulate wakefulness

VP also contains a small population of cholinergic neurons. Cholinergic neurons in the BF, adjacent to the VP, are known to regulate wakefulness,[24,25] and cortical EEG delta power.[26] However, whether VP^{ChAT} neurons regulate wakefulness and EEG power is unknown. To investigate the role of VP^{ChAT} neurons in sleep-wake regulation, we manipulated the neuronal activity of VP^{ChAT} neurons. First, we activated VP^{ChAT} neurons by chemogenetics in ChAT-Cre mice (Figures S1A and S1B). However, chemogenetic activation of VP^{ChAT} neurons did not alter sleep-wake stages or EEG power spectrum (Figures S1C–S2D). These results differed markedly from the chemogenetic activation of BF cholinergic neurons, which decreased cortical delta power.[26]

Optogenetic activation of BF cholinergic neurons is sufficient to induce an immediate transition from slow-wave sleep to wakefulness or REM sleep.[25] Therefore, we used optogenetics to stimulate VP^{ChAT} neurons in ChAT-Cre mice (Figure S2A). Activation of VP^{ChAT} neurons was confirmed by c-Fos labeling (Figure S2B).

However, optogenetic activation of VP^{ChAT} neurons at 20 Hz did not change sleep-wake stages or EEG power (Figures S2C–S2E). In total, we performed 38 trials of blue light stimulation in VP^{ChAT}-ChR2 mice and 39 trials in VP^{ChAT}-mCherry mice, but the percentage of wake, NREM, and REM sleep was not changed by stimulation (Figure S2F). One-hour optogenetic stimulation also did not change the amount of sleep (Figure S2G). These results indicate activation of VP^{ChAT} neurons did not increase arousal or alter EEG power, suggesting that VP^{ChAT} neurons are not involved in sleep-wake regulation, and further suggest that VP and BF play a different role in regulating wakefulness.

Activation of VP^{Vglut2} neurons facilitated anxiety/depressive-like behaviors

Next, we aimed to investigate the causal role of VP^{Vglut2} neurons in the control of depressive- and anxiety-like behaviors. Chemogenetics were used to activate or inhibit VP^{Vglut2} neurons in emotional behaviors. We found that chemogenetic activation of VP^{Vglut2} neurons did not alter locomotion in the open field test, but decreased the time spent in the center area (Figure 4A), indicating an anxiety-like behavior. Importantly, the immobility time was significantly increased in the TS and forced swimming tests upon chemogenetic activation of VP^{Vglut2} neurons (Figures 4B and 4C), suggesting that activation of VP^{Vglut2} neurons facilitates depressive-like behaviors. Furthermore, both time spent and entries in the open arms was decreased in the EPM test (Figure 4D), while time spent and entries in the white box were reduced in the black-white box test (Figure 4E). These results showed that activation of VP^{Vglut2} neurons induced anxiety/depressive-like behaviors. To further demonstrate the necessity of VP^{Vglut2} neurons in regulating emotion, we chemogenetically inhibited VP^{Vglut2} neurons. Chemogenetic inhibition of VP^{Vglut2} neurons did not alter locomotion in the open field test but increased the time spent in the center area (Figure 4F), suggesting a less anxiety-like status of mice. Importantly, the immobility time was significantly decreased in the TS and forced swimming tests (Figures 4G and 4H), suggesting that inhibition of VP^{Vglut2} neurons attenuated depressive-like behaviors. However, in the EPM test, time spent and entries in the open arms were not changed (Figure 4I), whereas in the black-white box test, only the entries, but not the total time spent in the white box, was increased (Figure 4J). Taken together, these data suggest that increasing the activity of VP^{Vglut2} neurons regulates emotional behaviors.

Parallel projections from VP^{Vglut2} neurons to LH and LHb

Having identified the role of VP^{Vglut2} neurons in regulating wakefulness and emotions, we next aimed to explore the circuit mechanisms. Using an AAV-based anterograde tracing, we found that VP^{Vglut2} neurons send very dense projections to the lateral hypothalamus (LH), LHb, VTA, and NAc (Figures S3A and S3B). Among them, LH and LHb are known brain regions that regulate arousal[5] and depression,[27–29] respectively. It is worth mentioning that mCherry was only expressed to VP^{Vglut2} neurons and the strong mCherry fluorescence in the NAc and adjacent BF regions is from the projection of VP neurons, but not the cell body. To further confirm VP-LH and VP-LHb projections, we used cholera toxin subunit B (CTB) based retrograde tracing. CTB-488 and CTB-647 were injected unilaterally into the LH and LHb, respectively. As a result, cells labeled with CTB-488 and CTB-647 were found in the VP, indicating that VP neurons project to both regions. Notably, approximately 65.5% of labeled VP neurons were LH-projecting and approximately 46.5% of labeled VP neurons were LHb-projecting. Interestingly, approximately 12.1% of VP neurons sent projections to both LH and LHb, suggesting that VP regulates wakefulness and emotions may be through separated projections (Figure S3C). Therefore, we decided to investigate these two parallel VP projections in the regulation of wakefulness and depressive-like behaviors, respectively.

VP^{Vglut2}-LH projections promoted wakefulness

Using optogenetics, we stimulated the VP^{Vglut2}-LH pathway *in vivo* to illustrate whether VP^{Vglut2} neurons promote arousal through LH. The AAV-hSyn-DIO-ChR2-mCherry or AAV-hSyn-DIO-mCherry control construct was injected bilaterally into the VP of Vglut2-Cre mice with optic fibers implanted above the LH (Figure 5A). The virus was well expressed in the VP, and abundant of mCherry terminals from VP^{Vglut2} neurons were found in the LH (Figure 5B). *In vivo* optogenetic stimulation of VP^{Vglut2}-LH projections at 20 Hz induced an immediate transition from NREM sleep to wakefulness, as well as a decrease in EEG delta power with a concomitant increase in EMG activity (Figure 5C), indicating that stimulation of VP^{Vglut2}-LH projections induced behavioral arousal. Short latencies for sleep-to-wake transitions were observed during blue-light stimulation in the LH at frequencies of 20–30 Hz (Figure 5D). In total, we conducted 40 trials of optogenetic stimulation in VP^{Vglut2}-ChR2-LH mice. It was observed that mice awakened from NREM sleep in all of these trials, whereas VP^{VGlut2}-mCherry-LH control mice displayed awakening from NREM sleep in only 4 of the 42 trials (Figure 5E). In addition, chronic stimulation of VP^{Vglut2}-LH projections (5-ms pulses at

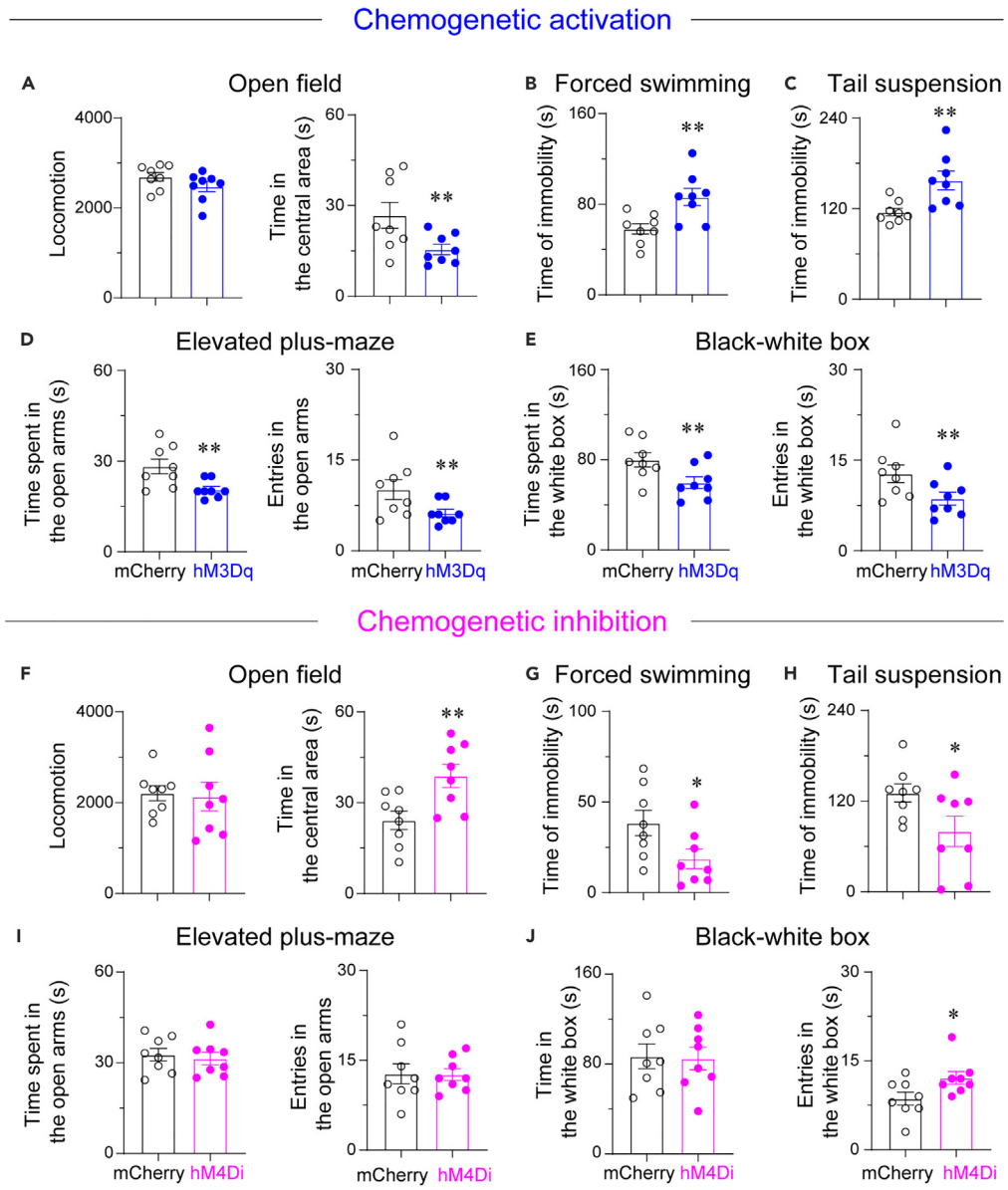

Figure 4. VP^{Vglut2} neurons exhibit activity-dependent regulation of depressive-like behaviors

(A) Chemogenetic activation of VP^{Vglut2} neurons did not affect locomotion, but decreased time spent in the center of the open field test. Time of immobility was increased after chemogenetic activation of VP^{Vglut2} neurons in both forced swimming (B) and TS (C) tests. (D) Chemogenetic activation of VP^{Vglut2} neurons decreased time spent and entries in the open arms of the EPM test. (E) Chemogenetic activation of VP^{Vglut2} neurons decreased time spent and entries in the white box of the black-white box test. n = 8 mice per group, **p < 0.01, unpaired *t*-test.

(F–J) Chemogenetic inhibition of VP glutamatergic neurons attenuated depressive-like behaviors. The following behavioral tests were used: open field (F), forced swimming (G), TS (H), EPM (I), and black-white box (J). n = 8 mice per group, *p < 0.05, **p < 0.01, unpaired *t*-test.

20 Hz, with 10-s ON/20-s OFF) for 1 h increased the amount of wakefulness, with a concomitant decrease in NREM and REM sleep (Figure 5F). This effect was stronger than optogenetic stimulation of VP cell bodies, which was only increased wakefulness for the first 30 min (Figure 2), suggesting that LH is the major downstream target for VP^{Vglut2} neurons in promoting wakefulness.

To further dissect the circuit mechanism of VP^{Vglut2}-LH projections in regulating wakefulness, we injected the AAV-hSyn-DIO-ChR2-mCherry construct into the VP of Vglut2-Cre:GAD67-GFP double-transgenic

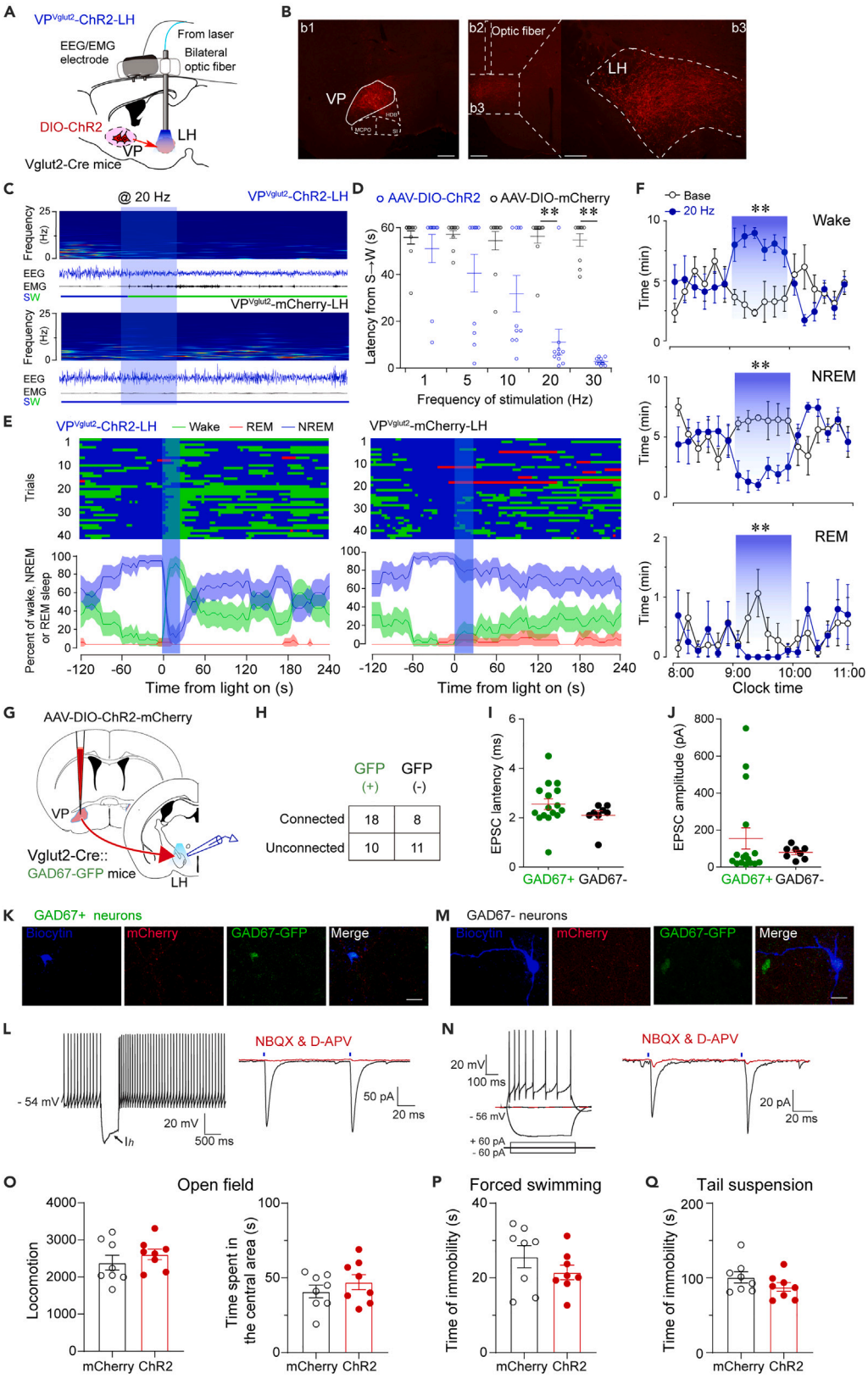
A
VP^Vglut2-ChR2-LH
From laser
EEG/EMG electrode
Bilateral optic fiber
DIO-ChR2
LH
VP
Vglut2-Cre mice
B
b1
VP
b2
Optic fiber
b3
LH
C
@ 20 Hz
VP^Vglut2-ChR2-LH
Frequency (Hz)
EEG
EMG
SW
VP^Vglut2-mCherry-LH
D
AAV-DIO-ChR2
AAV-DIO-mCherry
Latency from S→W (s)
Frequency of stimulation (Hz)
E
VP^Vglut2-ChR2-LH
Wake
REM
NREM
VP^Vglut2-mCherry-LH
Trials
Percent of wake, NREM or REM sleep
Time from light on (s)
F
Base
20 Hz
Wake
NREM
REM
Time (min)
Clock time
G
AAV-DIO-ChR2-mCherry
VP
Vglut2-Cre::
GAD67-GFP mice
LH
H
GFP (+)
GFP (-)
Connected 18 8
Unconnected 10 11
I
EPSC lantency (ms)
GAD67+ GAD67-
J
EPSC amplitude (pA)
GAD67+ GAD67-
K
GAD67+ neurons
Biocytin
mCherry
GAD67-GFP
Merge
M
GAD67- neurons
Biocytin
mCherry
GAD67-GFP
Merge
L
NBQX & D-APV
- 54 mV
20 mV
500 ms
Ih
50 pA
20 ms
N
NBQX & D-APV
20 mV
100 ms
- 56 mV
+ 60 pA
- 60 pA
20 pA
20 ms
O
Open field
Locomotion
mCherry ChR2
Time spent in the central area (s)
mCherry ChR2
P
Forced swimming
Time of immobility (s)
mCherry ChR2
Q
Tail suspension
Time of immobility (s)
mCherry ChR2

Figure 5. Optogenetic activation of VP^{Vglut2}-LH pathway increases wakefulness

(A) Schematic showing *in vivo* optogenetic stimulation of VP^{Vglut2}-LH projections in Vglut2-Cre mice. AAV-DIO-hSyn-ChR2-mCherry construct was bilaterally expressed in the VP, and two optical fibers that were used for LH light delivery were implanted.

(B) Representative images showing that ChR2-mCherry-positive cell bodies in the VP (b1), and the tip of fiber optic above the LH (b2). Dense axonal terminals of VP^{Vglut2} neurons were found in the LH (b3). Scale bars = 100 μm.

(C) EEG/EMG traces and EEG heatmap showed that optogenetic activation of VP^{Vglut2}-LH pathway induced wakefulness in ChR2 mice, but not mCherry control mice.

(D) Latencies of transitions from NREM sleep to wakefulness after optogenetic stimulation at different frequencies. $^{**}p < 0.01$, unpaired *t*-test.

(E) Sleep stage after blue-light stimulation. For each stimulation trial, EEG was analyzed for 6 min with a 2-min baseline, and the light-on time was 20 s at 20 Hz. The percentages of NREM sleep, REM sleep, and wakefulness were analyzed during the short-stimulation experiment.

(F) One-hour optogenetic stimulation of VP^{Vglut2}-LH pathway increased the amount of wakefulness but decreased NREM sleep and REM sleep during the inactive period. n = 5 mice, $^{**}p < 0.01$ using repeated-measures ANOVA, followed by paired *t*-test.

(G) Diagram for *in vitro* optogenetic stimulation of VP^{Vglut2}-LH pathway.

(H) Proportions of connected and unconnected GFP+ and GFP- neurons (n = 28 GFP+ neurons, n = 19 GFP- neurons, from 8 mice. Chi-square test; p = 0.1506).

(I and J) Latency (I) and amplitude (J) of light-evoked EPSCs in LH GFP+ and GFP- neurons.

(K) Typical example of a biocytin-labeled neuron (blue) that was GFP positive and responsive to light stimulation. Scale bar = 20 μm. (L) Electrophysiological properties of a GFP+ cell in the LH (left). Light-evoked postsynaptic currents were EPSCs, which were blocked by AMPA and NMDA receptor antagonists, NBQX and D-APV (right).

(M) Typical example of a biocytin-labeled neuron (blue) that was GFP negative and responsive to light stimulation. Scale bar = 20 μm.

(N) Electrophysiological properties of a GFP negative cell in the LH (left). Light-evoked postsynaptic currents were EPSCs (right).

(O) Optogenetic activation of VP^{Vglut2}-LH projections did not alter locomotion and time spent in the center area in the open field test. n = 8 mice per group, p > 0.05, unpaired *t*-test.

(P and Q) Optogenetic activation of VP^{Vglut2}-LH projections did not alter immobility time in the forced swimming (P) and TS (Q) tests. n = 8 mice per group, p > 0.05, unpaired *t*-test.

mice and then recorded the activity of LH neurons under blue-light stimulation in acute slices *in vitro* (Figure 5G). Previous studies have shown that LH GABAergic neurons and non-GABAergic Vglut2+ neurons are wake-promoting.[30,31] Here, we divided LH neurons into two subtypes: GFP+ (putative GABAergic) neurons and GFP- (putative non-GABAergic) neurons, to explore whether VP^{Vglut2} neurons promote wakefulness by activating one of them. Interestingly, VP^{Vglut2} neurons innervated slightly more LH GABAergic neurons, but no statistical difference (Figure 5H, p = 0.1506). LH neurons received excitatory postsynaptic currents (EPSCs) from VP^{Vglut2} neurons, but the latency and amplitude did not differ between GABAergic neurons and non-GABAergic neurons (Figures 5I and 5J). Because the latency of EPSCs was less than 5 ms, we suspected that VP^{Vglut2} neurons directly innervate both LH GABAergic and non-GABAergic neurons. Optogenetic stimulation of axonal terminals of VP glutamatergic neurons in the LH evoked EPSCs in both GABAergic neurons (Figures 5K and 5L) and non-GABAergic neurons (Figures 5M and 5N), which were blocked by the AMPA and NMDA receptor antagonists, NBQX and D-APV. We also explored whether VP^{Vglut2}-LH projections regulate anxiety/depressive-like behaviors. As a result, optogenetic activation of VP^{Vglut2}-LH projections did not induce anxiety/depressive-like behaviors, with a very slight trend to decrease immobility time in forced swimming and TS tests (Figures 5O–5Q).

Taken together, VP^{Vglut2}-LH projections promote wakefulness, which may be mediated by LH GABAergic and non-GABAergic neurons.

VP^{Vglut2}-LHb projections induced depressive-like behaviors

Previous studies showed that excitatory inputs induced hyperactivity of LHb neurons resulting in depressive-like behaviors,[27–29] thus, we want to investigate whether LHb mediates activation of VP^{Vglut2} neurons-induced depressive-like behaviors. AAV-hSyn-DIO-ChR2-mCherry or AAV-hSyn-DIO-mCherry control construct was injected bilaterally into the VP of Vglut2-Cre mice with implantation of optic fibers bilaterally above the LHb (Figures 6A and 6B). Optogenetic stimulation VP^{Vglut2}-LHb projections increased c-Fos expression in the LHb (Figure 6C), indicating that stimulation of VP^{Vglut2}-LHb projections increased the LHb neuronal activity. *In vitro* electrophysiological recording showed that VP^{Vglut2} neurons release glutamate to LHb neurons, mediated by AMPA and NMDA receptors (Figures 6D and 6E). Optogenetic stimulation of VP^{Vglut2}-LHb projections

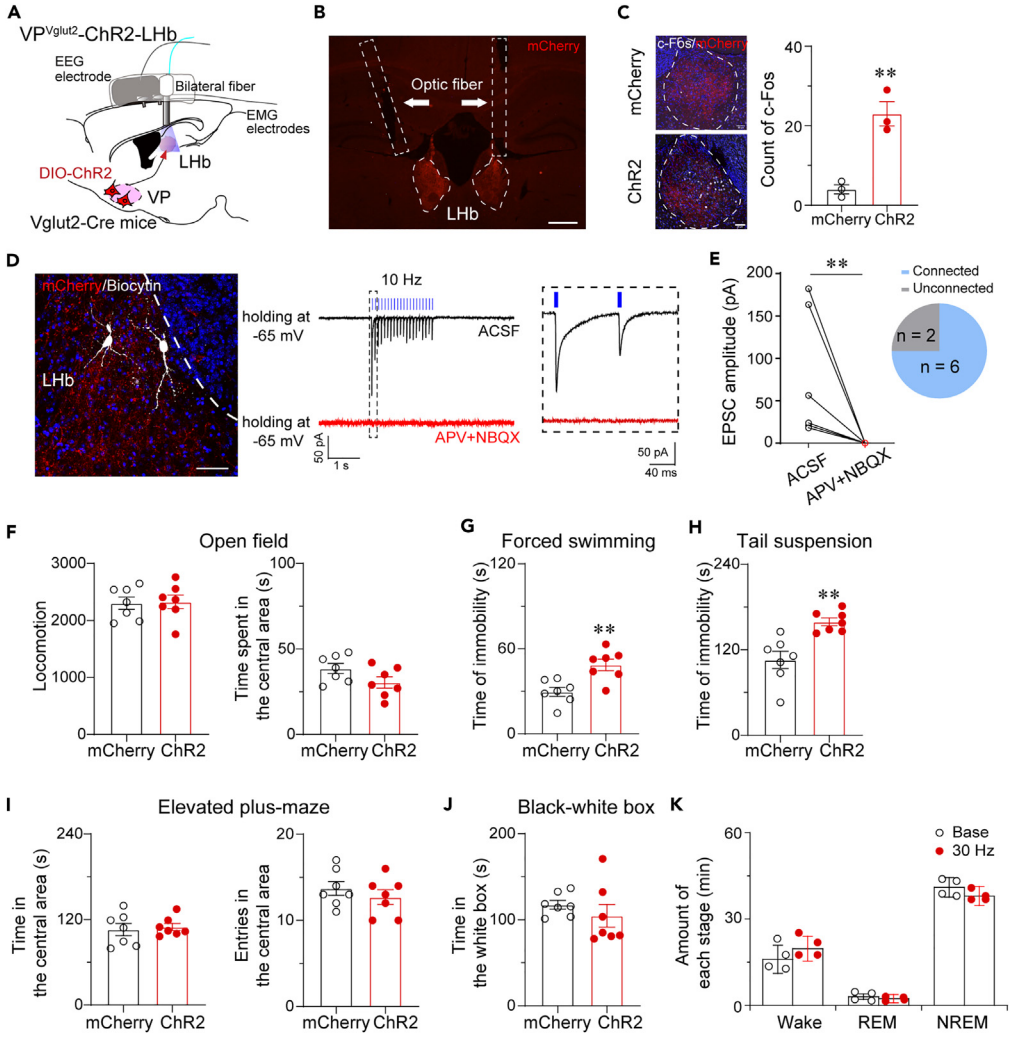

Figure 6. Optogenetic activation of VP^{Vglut2}-LHb pathway facilitates depressive-like behaviors

(A) Schematic showing *in vivo* optogenetic stimulation of VP^{Vglut2}-LHb projections in Vglut2-Cre mice.

(B) Dense axonal terminals of VP^{Vglut2} neurons were found in the LHb. Arrows indicate the tracks of bilaterally implanted optic fibers. Scale bar = 100 μm.

(C) Optogenetic stimulation increased c-Fos expression in the LHb in Vglut2-Cre mice transduced with ChR2 in the VP, and quantification of c-Fos immunoreactivity in the LHb following light stimulation. n = 3 mice per group, **p < 0.01, unpaired *t*-test. Scale bars = 50 μm.

(D and E) Glutamatergic transmutation from VP^{Vglut2}-LHb via AMPAR and NMDAR was identified by *in vitro* slice recording. (D) Left: A representative image showing that two connected biocytin-filled neurons (white) were located in the LHb. Scale bar = 100 μm. Right: Sample traces of optogenetically generated EPSCs in a LHb neuron. (E) Amplitude of light-evoked EPSCs. 6 out of 8 recorded LHb cells were responsive to light application. **p < 0.01, paired *t*-test.

(F) Optogenetic activation of VP^{Vglut2}-LHb projections did not alter locomotion and time spent in the center area in the open field test.

(G and H) Optogenetic activation of VP^{Vglut2}-LHb projections increased the time of immobility in the forced swimming (G) and TS (H) tests. (I and J) Optogenetic activation of VP^{Vglut2}-LHb projections did not alter performance in the EPM and black-white box tests. n = 7 mice per group, **p < 0.01, unpaired *t*-test.

(K) Optogenetic activation of VP^{Vglut2}-LHb projections did not alter sleep-wake amount. n = 4 mice, paired *t*-test.

in vivo did not alter the locomotion and time spent in the central area in the open field test (Figure 6F), but significantly increased the immobility time in forced swimming and TS tests (Figures 6G and 6H). In addition, optogenetic stimulation of VP^{Vglut2}-LHb projections did not change behaviors in the EPM and black-white box tests (Figures 6I and 6J). Moreover, optogenetic stimulation of VP^{Vglut2}-LHb projections did not affect the

amount of sleep and wakefulness (Figure 6K), suggesting that the VP^{Vglut2}-LHb pathway is only involved in the regulation of depressive-like behaviors.

DISCUSSION

Behavioral arousal refers to the state of increased wakefulness, which is closely linked to motivation and reward,[32,33] while depression and anxiety are also associated with altered arousal.[34] Our results demonstrated that activation of VP^{Vglut2} neurons induced wakefulness and anxiety/depressive-like behaviors, which could potentially be relevant as individuals with MDD often experience symptoms of insomnia. The rational role of VP^{Vglut2} neurons in regulating wakefulness and emotions was suggested by the fact that *in vivo* calcium activity of VP^{Vglut2} neurons was increased during both wakefulness and anxiety/depressive-like behaviors (Figure S4A). The bidirectional activity manipulation of VP^{Vglut2} neurons demonstrates the causal role of these neurons in regulating wakefulness and anxiety/depressive-like behaviors (Figure S4B). Importantly, we have dissected two parallel pathways from VP^{Vglut2} neurons in regulating arousal and depressive behaviors: VP^{Vglut2}-LH projections promoted arousal, and VP^{Vglut2}-LHb projections promoted depressive-like behaviors (Figure S4C). Our results strongly suggest that glutamatergic neurons in the VP are a key node in the integrating of altered arousal and depressive-like behaviors through separated pathways.

As a key node in the ventral basal ganglia, the VP integrates inputs from NAc D_1R and D_2R neurons and sends outputs to LH, VTA, LHb, and back to NAc.[20,35] The VP plays a crucial role in the regulation of motivation,[11] reward seeking,[12–14,36] decision-making,[37] addiction,[38] stress,[15] behavioral avoidance,[39] and depression-related behaviors.[16,17] Glutamatergic and GABAergic VP neurons might mediate the opposing regulation of "positive" and "negative" behaviors. Raising lines of evidence support this idea: chemogenetic stimulation of glutamatergic VP neurons inhibits cocaine seeking in mice withdrawn from intravenous cocaine self-administration, whereas stimulation of GABAergic VP neurons enhances cocaine seeking.[39] Moreover, GABAergic VP neurons are essential for movements toward reward, whereas glutamatergic VP neurons are essential for movements to avoid a threat.[11] In addition, GABAergic VP neurons drive positive reinforcement, but glutamatergic VP neurons lead to behavioral avoidance.[40] Our recent study also supports this idea that activation of VP GABAergic neurons promotes wakefulness related to motivation, but activation of VP glutamatergic neurons induces wakefulness related to depression, reported in this study. On the other hand, the opposing contributions could also be due to the different projections.[16] PV neurons in the VP that project to either the LHb or VTA contribute to social withdrawal or behavioral despair, but not both, in depression. The GABAergic and glutamatergic neurons and their distinct projections suggest that the VP mediates several opposite but related behaviors, including motivation, reward, and depression, all based on normal or abnormal behavioral arousal.

The BF is adjacent to the VP and has similar subtypes of neurons, including glutamatergic, GABAergic, and cholinergic neurons. However, they differ in their roles in sleep-wake regulation. Chemogenetic and optogenetic activation of VP GABAergic neurons promoted wakefulness for 4 h by the disinhibition of midbrain dopaminergic neurons.[7] However, chemogenetic activation of GABAergic BF neurons increased wakefulness for 13 h,[41] but optogenetic activation of BF somatostatin positive neurons promoted sleep.[24] Optogenetic stimulation of glutamatergic VP neurons at a frequency over 20 Hz increased behavioral arousal but was not as strong as the effect induced by optogenetic stimulation of VP GABAergic neurons. Chemogenetic activation of glutamatergic BF neurons had little effect on sleep-wake cycles or EEG power density,[41] but optogenetic activation of glutamatergic BF neurons at 10 Hz induced a marked increase in wakefulness.[24] Interestingly, a loss-of-function study of lesioning of glutamatergic BF neurons also increased wakefulness in the dark phase,[42] which is markedly different from chemogenetic inhibition of glutamatergic VP neurons, which slightly increased NREM sleep. Finally, cholinergic VP neurons had little effect on sleep-wake regulation, but cholinergic BF neurons strongly inhibited the delta power of cortical EEG,[26] and induced wakefulness.[24,25,41] Taken together, VP and BF play significantly different roles in sleep-wake regulation despite being adjacent brain regions and having similar subtypes of neurons, probably because of their distinct local interactions and long-range connections, as well as because they are involved in the regulation of different behaviors.[20,43–45]

Higher brain functions, including motivation, reward, feeding, and learning, are associated with heightened arousal, while psychiatric disorders involve dysfunctions in sleep-wake regulation, including insomnia.[46–49] Depression severity is associated with the severity of insomnia, and the presence of one disorder is a risk factor for the development of the other disorder.[50] Thus, the treatment of insomnia and

depression may prevent relapse in patients with co-morbid MDD and insomnia. Our study provides strong evidence that aberrant activation of glutamatergic VP neurons leads to depressive-related insomnia. Disruption of this aberrant activation prevents insomnia and depressive-like behaviors. Meanwhile, disturbances of REM sleep are typical for most depressed patients.[51] In our study, we found increased activity of VP glutamatergic neurons in REM sleep while inhibition of VP glutamatergic neurons decreased theta power in the REM sleep. These results suggest that REM sleep and depressive-behaviors are linked and associated with activity of VP glutamatergic neurons. The VP may be an important target in treating depression. In future studies, we will further identify how the subpopulation of LH- and LHb-projecting glutamatergic VP neurons regulate insomnia related to depression.

In summary, our findings showed that separate projections of glutamatergic VP neurons regulate wakefulness and emotions through the LH and LHb.

Limitations of the study

There are several limitations in this study. First, we did not specifically investigate whether VP glutamatergic neurons regulate wakefulness-related depression. While the regulation of VP glutamatergic neurons affects wakefulness and emotions, it remains unclear whether the wakefulness is associated with depression. In future studies, we intend to suppress VP glutamatergic neurons to alleviate insomnia in a depressive model. Second, it is necessary to determine whether glutamatergic VP neurons projecting to the LH and LHb are completely separate entities, or if there are VP neurons that project to both regions and jointly regulate wakefulness in relation to depression. Third, we have not investigated whether there are other downstream regions influenced by VP glutamatergic neurons that might also play a role in regulating wakefulness and emotion (for example, the VTA). These regions should be examined to gain a comprehensive understanding of the neural circuitry involved.

STAR★METHODS

Detailed methods are provided in the online version of this paper and include the following:

- KEY RESOURCES TABLE
- RESOURCE AVAILABILITY
  - Lead contact
  - Materials availability
  - Data and code availability
- EXPERIMENTAL MODEL AND STUDY PARTICIPANT DETAILS
  - Experimental animals
- METHOD DETAILS
  - EEG/EMG electrode-implantation surgery
  - EEG recordings and analysis
  - Viral injections and fiber implantations
  - Fiber photometry
  - Optogenetic stimulation *in vivo*
  - Behavioral tests
  - Immunohistochemistry
  - *In vitro* electrophysiology
- QUANTIFICATION AND STATISTICAL ANALYSIS

SUPPLEMENTAL INFORMATION

Supplemental information can be found online at https://doi.org/10.1016/j.isci.2023.107385.

ACKNOWLEDGMENTS

We thank Dr. Brent Asrican (University of North Carolina at Chapel Hill) for language editing. This study was supported by the National Key Research and Development Program of China (Grant numbers 2020YFC2005300, 2021YFC2501400 to W-M.Q.), the STI2030-Major Project (2021ZD0203400 to Z-L.H.), the National Natural Science Foundation of China (82020108014 and 32070984 to Z-L.H.; 82071491 and 31871072 to W-M.Q.), the Shanghai Science and Technology Innovation Action Plan Laboratory Animal Research Project (201409001800 to Z-L.H.), Shanghai Municipal Science and Technology Major Project

(2018SHZDZX01 to Z-L.H.), ZJ Lab Program for Shanghai Outstanding Academic Leaders (to Z-L.H.), and Shanghai Center for Brain Science and Brain-Inspired Technology and Lingang Laboratory & National Key Laboratory of Human Factors Engineering Joint Grant (LG-TKN-202203-01). Y-D.L. was supported in part by start-up funding of Shanghai Jiao Tong University. M.L. was supported in part by funding from the Japan Society for the Promotion of Science (JP21H02802 and JP22K21351), the Japan Agency for Medical Research and Development (AMED) (JP21zf0127005) and the Ministry of Education, Culture, Sports, Science and Technology (MEXT) of Japan (JP23H04148).

AUTHOR CONTRIBUTIONS

Y-D.L., Y-J.L., and Z-L.H. conceived the project. Y-J.L., Y-D.L., W-M.Q., and Z-L.H. designed the experiments. Y-J.L., Y-D.L., J.G., Z-K.C. and Z-L.L. performed all experiments and collected and analyzed the data. Y-D.L. and Y-J.L. wrote the manuscript. W-M.Q. and Z-L.H. mentored the project, M.L. discussed the project and helped draft the manuscript, and all of the authors discussed the manuscript.

DECLARATION OF INTERESTS

The authors declare that they have no conflict of interest.

Received: June 26, 2023
Revised: June 30, 2023
Accepted: July 11, 2023
Published: August 5, 2023

REFERENCES

1. Ohayon, M.M. (2002). Epidemiology of insomnia: what we know and what we still need to learn. Sleep Med. Rev. *6*, 97–111. https://doi.org/10.1053/smrv.2002.0186.

2. Stewart, R., Besset, A., Bebbington, P., Brugha, T., Lindesay, J., Jenkins, R., Singleton, N., and Meltzer, H. (2006). Insomnia comorbidity and impact and hypnotic use by age group in a national survey population aged 16 to 74 years. Sleep *29*, 1391–1397. https://doi.org/10.1093/sleep/29.11.1391.

3. Vargas, I., and Perlis, M.L. (2020). Insomnia and depression: clinical associations and possible mechanistic links. Curr. Opin. Psychol. *34*, 95–99. https://doi.org/10.1016/j.copsyc.2019.11.004.

4. Li, Y., Bao, H., Luo, Y., Yoan, C., Sullivan, H.A., Quintanilla, L., Wickersham, I., Lazarus, M., Shih, Y.Y.I., and Song, J. (2020). Supramammillary nucleus synchronizes with dentate gyrus to regulate spatial memory retrieval through glutamate release. Elife *9*, 53129. ARTN e53129. https://doi.org/10.7554/eLife.

5. Arrigoni, E., Chee, M.J.S., and Fuller, P.M. (2019). To eat or to sleep: That is a lateral hypothalamic question. Neuropharmacology *154*, 34–49. https://doi.org/10.1016/j.neuropharm.2018.11.017.

6. Stuber, G.D., and Wise, R.A. (2016). Lateral hypothalamic circuits for feeding and reward. Nat. Neurosci. *19*, 198–205. https://doi.org/10.1038/nn.4220.

7. Li, Y.D., Luo, Y.J., Xu, W., Ge, J., Cherasse, Y., Wang, Y.Q., Lazarus, M., Qu, W.M., and Huang, Z.L. (2021). Ventral pallidal GABAergic neurons control wakefulness associated with motivation through the ventral tegmental pathway. Mol. Psychiatr. *26*, 2912–2928. https://doi.org/10.1038/s41380-020-00906-0.

8. Luo, Y.J., Li, Y.D., Wang, L., Yang, S.R., Yuan, X.S., Wang, J., Cherasse, Y., Lazarus, M., Chen, J.F., Qu, W.M., and Huang, Z.L. (2018). Nucleus accumbens controls wakefulness by a subpopulation of neurons expressing dopamine D1 receptors. Nat. Commun. *9*, 1576. https://doi.org/10.1038/s41467-018-03889-3.

9. Yon, A., Scogin, F., DiNapoli, E.A., McPherron, J., Arean, P.A., Bowman, D., Jamison, C.S., Karpe, J.A., Latour, D., Reynolds, C.F., 3rd, et al. (2014). Do manualized treatments for depression reduce insomnia symptoms? J. Clin. Psychol. *70*, 616–630. https://doi.org/10.1002/jclp.22062.

10. Gebara, M.A., Siripong, N., DiNapoli, E.A., Maree, R.D., Germain, A., Reynolds, C.F., Kasckow, J.W., Weiss, P.M., and Karp, J.F. (2018). Effect of insomnia treatments on depression: A systematic review and meta-analysis. Depress. Anxiety *35*, 717–731. https://doi.org/10.1002/da.22776.

11. Stephenson-Jones, M., Bravo-Rivera, C., Ahrens, S., Furlan, A., Xiao, X., Fernandes-Henriques, C., and Li, B. (2020). Opposing Contributions of GABAergic and Glutamatergic Ventral Pallidal Neurons to Motivational Behaviors. Neuron *105*, 921–933.e5. https://doi.org/10.1016/j.neuron.2019.12.006.

12. Creed, M., Ntamati, N.R., Chandra, R., Lobo, M.K., and Lüscher, C. (2016). Convergence of Reinforcing and Anhedonic Cocaine Effects in the Ventral Pallidum. Neuron *92*, 214–226. https://doi.org/10.1016/j.neuron.2016.09.001.

13. Ottenheimer, D., Richard, J.M., and Janak, P.H. (2018). Ventral pallidum encodes relative reward value earlier and more robustly than nucleus accumbens. Nat. Commun. *9*, 4350. https://doi.org/10.1038/s41467-018-06849-z.

14. Ottenheimer, D.J., Bari, B.A., Sutlief, E., Fraser, K.M., Kim, T.H., Richard, J.M., Cohen, J.Y., and Janak, P.H. (2020). A quantitative reward prediction error signal in the ventral pallidum. Nat. Neurosci. *23*, 1267–1276. https://doi.org/10.1038/s41593-020-0688-5.

15. Chang, C.H., and Grace, A.A. (2014). Amygdala-ventral pallidum pathway decreases dopamine activity after chronic mild stress in rats. Biol. Psychiatr. *76*, 223–230. https://doi.org/10.1016/j.biopsych.2013.09.020.

16. Knowland, D., Lilascharoen, V., Pacia, C.P., Shin, S., Wang, E.H.J., and Lim, B.K. (2017). Distinct Ventral Pallidal Neural Populations Mediate Separate Symptoms of Depression. Cell *170*, 284–297.e18. https://doi.org/10.1016/j.cell.2017.06.015.

17. Wade, B.S., Joshi, S.H., Njau, S., Leaver, A.M., Vasavada, M., Woods, R.P., Gutman, B.A., Thompson, P.M., Espinoza, R., and Narr, K.L. (2016). Effect of Electroconvulsive Therapy on Striatal Morphometry in Major Depressive Disorder. Neuropsychopharmacology *41*, 2481–2491. https://doi.org/10.1038/npp.2016.48.

18. Ji, M.J., Zhang, X.Y., Chen, Z., Wang, J.J., and Zhu, J.N. (2019). Orexin prevents depressive-like behavior by promoting stress resilience. Mol. Psychiatr. *24*, 282–293. https://doi.org/10.1038/s41380-018-0127-0.

19. Oishi, Y., Xu, Q., Wang, L., Zhang, B.J., Takahashi, K., Takata, Y., Luo, Y.J., Cherasse, Y., Schiffmann, S.N., de Kerchove d'Exaerde, A., et al. (2017). Slow-wave sleep is controlled

by a subset of nucleus accumbens core neurons in mice. Nat. Commun. *8*, 734. https://doi.org/10.1038/s41467-017-00781-4.

20. Root, D.H., Melendez, R.I., Zaborszky, L., and Napier, T.C. (2015). The ventral pallidum: Subregion-specific functional anatomy and roles in motivated behaviors. Prog. Neurobiol. *130*, 29–70. https://doi.org/10.1016/j.pneurobio.2015.03.005.

21. Eban-Rothschild, A., Giardino, W.J., and de Lecea, L. (2017). To sleep or not to sleep: neuronal and ecological insights. Curr. Opin. Neurobiol. *44*, 132–138. https://doi.org/10.1016/j.conb.2017.04.010.

22. Riemann, D., Berger, M., and Voderholzer, U. (2001). Sleep and depression–results from psychobiological studies: an overview. Biol. Psychol. *57*, 67–103. https://doi.org/10.1016/s0301-0511(01)00090-4.

23. Li, Y.D., Luo, Y.J., Chen, Z.K., Quintanilla, L., Cherasse, Y., Zhang, L., Lazarus, M., Huang, Z.L., and Song, J. (2022). Hypothalamic modulation of adult hippocampal neurogenesis in mice confers activity-dependent regulation of memory and anxiety-like behavior. Nat. Neurosci. *25*, 630–645. https://doi.org/10.1038/s41593-022-01065-x.

24. Xu, M., Chung, S., Zhang, S., Zhong, P., Ma, C., Chang, W.C., Weissbourd, B., Sakai, N., Luo, L., Nishino, S., and Dan, Y. (2015). Basal forebrain circuit for sleep-wake control. Nat. Neurosci. *18*, 1641–1647. https://doi.org/10.1038/nn.4143.

25. Han, Y., Shi, Y.F., Xi, W., Zhou, R., Tan, Z.B., Wang, H., Li, X.M., Chen, Z., Feng, G., Luo, M., et al. (2014). Selective activation of cholinergic basal forebrain neurons induces immediate sleep-wake transitions. Curr. Biol. *24*, 693–698. https://doi.org/10.1016/j.cub.2014.02.011.

26. Chen, L., Yin, D., Wang, T.X., Guo, W., Dong, H., Xu, Q., Luo, Y.J., Cherasse, Y., Lazarus, M., Qiu, Z.L., et al. (2016). Basal forebrain cholinergic neurons primarily contribute to inhibition of electroencephalogram delta activity; rather than inducing behavioral wakefulness in mice. Neuropsychopharmacology *41*, 2133–2146. https://doi.org/10.1038/npp.2016.13.

27. Lin, S., Huang, L., Luo, Z.C., Li, X., Jin, S.Y., Du, Z.J., Wu, D.Y., Xiong, W.C., Huang, L., Luo, Z.Y., et al. (2022). The ATP level in the medial prefrontal cortex regulates depressive-like behavior via the medial prefrontal cortex-lateral habenula pathway. Biol. Psychiatr. *92*, 179–192. https://doi.org/10.1016/j.biopsych.2022.02.014.

28. Zheng, Z., Guo, C., Li, M., Yang, L., Liu, P., Zhang, X., Liu, Y., Guo, X., Cao, S., Dong, Y., et al. (2022). Hypothalamus-habenula potentiation encodes chronic stress experience and drives depression onset. Neuron *110*, 1400–1415.e6. https://doi.org/10.1016/j.neuron.2022.01.011.

29. Cui, Y., Huang, X., Huang, P., Huang, L., Feng, Z., Xiang, X., Chen, X., Li, A., Ren, C., and Li, H. (2022). Reward ameliorates depressive-like behaviors via inhibition of the substantia innominata to the lateral habenula projection. Sci. Adv. *8*, eabn0193. https://doi.org/10.1126/sciadv.abn0193.

30. Venner, A., Anaclet, C., Broadhurst, R.Y., Saper, C.B., and Fuller, P.M. (2016). A Novel Population of Wake-Promoting GABAergic Neurons in the Ventral Lateral Hypothalamus. Curr. Biol. *26*, 2137–2143. https://doi.org/10.1016/j.cub.2016.05.078.

31. Wang, R.F., Guo, H., Jiang, S.Y., Liu, Z.L., Qu, W.M., Huang, Z.L., and Wang, L. (2021). Control of wakefulness by lateral hypothalamic glutamatergic neurons in male mice. J. Neurosci. Res. *99*, 1689–1703. https://doi.org/10.1002/jnr.24828.

32. Harmon-Jones, E., and Winkielman, P. (2007). Social Neuroscience : Integrating Biological and Psychological Explanations of Social Behavior (Guilford Press).

33. Jones, B.E. (2003). Arousal systems. Front. Biosci. *8*, s438–s451. https://doi.org/10.2741/1074.

34. Bowrey, H.E., James, M.H., and Aston-Jones, G. (2017). New directions for the treatment of depression: Targeting the photic regulation of arousal and mood (PRAM) pathway. Depress. Anxiety *34*, 588–595. https://doi.org/10.1002/da.22635.

35. Kupchik, Y.M., Brown, R.M., Heinsbroek, J.A., Lobo, M.K., Schwartz, D.J., and Kalivas, P.W. (2015). Coding the direct/indirect pathways by D_1 and D_2 receptors is not valid for accumbens projections. Nat. Neurosci. *18*, 1230–1232. Epub 2015 Jul 27. https://doi.org/10.1038/nn.4068.

36. Tooley, J., Marconi, L., Alipio, J.B., Matikainen-Ankney, B., Georgiou, P., Kravitz, A.V., and Creed, M.C. (2018). Glutamatergic Ventral Pallidal Neurons Modulate Activity of the Habenula-Tegmental Circuitry and Constrain Reward Seeking. Biol. Psychiatr. *83*, 1012–1023. https://doi.org/10.1016/j.biopsych.2018.01.003.

37. Ottenheimer, D.J., Wang, K., Tong, X., Fraser, K.M., Richard, J.M., and Janak, P.H. (2020). Reward activity in ventral pallidum tracks satiety-sensitive preference and drives choice behavior. Sci. Adv. *6*, eabc9321. ARTN eabc9321. https://doi.org/10.1126/sciadv.abc9321.

38. James, M.H., and Aston-Jones, G. (2016). The Ventral Pallidum: Proposed Integrator of Positive and Negative Factors in Cocaine Abuse. Neuron *92*, 5–8. https://doi.org/10.1016/j.neuron.2016.09.042.

39. Heinsbroek, J.A., Bobadilla, A.C., Dereschewitz, E., Assali, A., Chalhoub, R.M., Cowan, C.W., and Kalivas, P.W. (2020). Opposing Regulation of Cocaine Seeking by Glutamate and GABA Neurons in the Ventral Pallidum. Cell Rep. *30*, 2018–2027.e3. https://doi.org/10.1016/j.celrep.2020.01.023.

40. Faget, L., Zell, V., Souter, E., McPherson, A., Ressler, R., Gutierrez-Reed, N., Yoo, J.H., Dulcis, D., and Hnasko, T.S. (2018). Opponent control of behavioral reinforcement by inhibitory and excitatory projections from the ventral pallidum. Nat. Commun. *9*, 849. https://doi.org/10.1038/s41467-018-03125-y.

41. Anaclet, C., Pedersen, N.P., Ferrari, L.L., Venner, A., Bass, C.E., Arrigoni, E., and Fuller, P.M. (2015). Basal forebrain control of wakefulness and cortical rhythms. Nat. Commun. *6*, 8744. https://doi.org/10.1038/ncomms9744.

42. Peng, W., Wu, Z., Song, K., Zhang, S., Li, Y., and Xu, M. (2020). Regulation of sleep homeostasis mediator adenosine by basal forebrain glutamatergic neurons. Science *369*, eabb0556. ARTN eabb0556 10.1126/science.abb0556.

43. Prasad, A.A., Xie, C., Chaichim, C., Nguyen, J.H., McClusky, H.E., Killcross, S., Power, J.M., and McNally, G.P. (2020). Complementary Roles for Ventral Pallidum Cell Types and Their Projections in Relapse. J. Neurosci. *40*, 880–893. https://doi.org/10.1523/JNEUROSCI.0262-19.2019.

44. Golden, S.A., Heshmati, M., Flanigan, M., Christoffel, D.J., Guise, K., Pfau, M.L., Aleyasin, H., Menard, C., Zhang, H., Hodes, G.E., et al. (2016). Basal forebrain projections to the lateral habenula modulate aggression reward. Nature *534*, 688–692. https://doi.org/10.1038/nature18601.

45. Agostinelli, L.J., Geerling, J.C., and Scammell, T.E. (2019). Basal forebrain subcortical projections. Brain Struct. Funct. *224*, 1097–1117. https://doi.org/10.1007/s00429-018-01820-6.

46. Lazarus, M., Huang, Z.L., Lu, J., Urade, Y., and Chen, J.F. (2012). How do the basal ganglia regulate sleep-wake behavior? Trends Neurosci. *35*, 723–732. https://doi.org/10.1016/j.tins.2012.07.001.

47. Russo, S.J., and Nestler, E.J. (2013). The brain reward circuitry in mood disorders. Nat. Rev. Neurosci. *14*, 609–625. https://doi.org/10.1038/nrn3381.

48. Wulff, K., Gatti, S., Wettstein, J.G., and Foster, R.G. (2010). Sleep and circadian rhythm disruption in psychiatric and neurodegenerative disease. Nat. Rev. Neurosci. *11*, 589–599. https://doi.org/10.1038/nrn2868.

49. Polunina, A.G., and Davydov, D.M. (2004). EEG spectral power and mean frequencies in early heroin abstinence. Prog. Neuro-Psychopharmacol. Biol. Psychiatry *28*, 73–82. https://doi.org/10.1016/j.pnpbp.2003.09.022.

50. Franzen, P.L., and Buysse, D.J. (2008). Sleep disturbances and depression: risk relationships for subsequent depression and therapeutic implications. Dialogues Clin. Neurosci. *10*, 473–481.

51. Wang, Y.Q., Li, R., Zhang, M.Q., Zhang, Z., Qu, W.M., and Huang, Z.L. (2015). The Neurobiological Mechanisms and Treatments of REM Sleep Disturbances in Depression. Curr. Neuropharmacol. *13*, 543–553. https://doi.org/10.2174/1570159x13666150310002540.

52. Vong, L., Ye, C., Yang, Z., Choi, B., Chua, S., Jr., and Lowell, B.B. (2011). Leptin action on GABAergic neurons prevents obesity and reduces inhibitory tone to POMC neurons.

Neuron *71*, 142–154. https://doi.org/10.1016/j.neuron.2011.05.028.

53. Rossi, J., Balthasar, N., Olson, D., Scott, M., Berglund, E., Lee, C.E., Choi, M.J., Lauzon, D., Lowell, B.B., and Elmquist, J.K. (2011). Melanocortin-4 receptors expressed by cholinergic neurons regulate energy balance and glucose homeostasis. Cell Metabol. *13*, 195–204. https://doi.org/10.1016/j.cmet.2011.01.010.

54. Tamamaki, N., Yanagawa, Y., Tomioka, R., Miyazaki, J.I., Obata, K., and Kaneko, T. (2003). Green fluorescent protein expression and colocalization with calretinin, parvalbumin, and somatostatin in the GAD67-GFP knock-in mouse. J. Comp. Neurol. *467*, 60–79. https://doi.org/10.1002/cne.10905.

55. Huang, Z.L., Qu, W.M., Eguchi, N., Chen, J.F., Schwarzschild, M.A., Fredholm, B.B., Urade, Y., and Hayaishi, O. (2005). Adenosine A2A, but not A1, receptors mediate the arousal effect of caffeine. Nat. Neurosci. *8*, 858–859. https://doi.org/10.1038/nn1491.

56. Li, Y.D., Ge, J., Luo, Y.J., Xu, W., Wang, J., Lazarus, M., Hong, Z.Y., Qu, W.M., and Huang, Z.L. (2020). High cortical delta power correlates with aggravated allodynia by activating anterior cingulate cortex GABAergic neurons in neuropathic pain mice. Pain *161*, 288–299. https://doi.org/10.1097/j.pain.0000000000001725.

57. Wu, Y.E., Li, Y.D., Luo, Y.J., Wang, T.X., Wang, H.J., Chen, S.N., Qu, W.M., and Huang, Z.L. (2015). Gelsemine alleviates both neuropathic pain and sleep disturbance in partial sciatic nerve ligation mice. Acta Pharmacol. Sin. *36*, 1308–1317. https://doi.org/10.1038/aps.2015.86.

58. Chen, Z.K., Dong, H., Liu, C.W., Liu, W.Y., Zhao, Y.N., Xu, W., Sun, X., Xiong, Y.Y., Liu, Y.Y., Yuan, X.S., et al. (2022). A cluster of mesopontine GABAergic neurons suppresses REM sleep and curbs cataplexy. Cell Discov. *8*, 115. https://doi.org/10.1038/s41421-022-00456-5.

STAR★METHODS

KEY RESOURCES TABLE

REAGENT or RESOURCE	SOURCE	IDENTIFIER
Antibodies		
Rabbit polyclonal anti-Fos	Millipore	Cat#ABE457; RRID: AB_2631318
Alexa Fluor 488 Donkey anti-Rabbit	Invitrogen	Cat #A32790
streptavidin conjugated to Alexa 405	Invitrogen	S11223
streptavidin conjugated to Alexa 647	Invitrogen	S32357
Bacterial and virus strains		
AAV2/9-hSyn-DIO-hM3Dq-mCherry	Taitool Bioscience	Cat #S0192-9
AAV2/9-hSyn-DIO-hM4Di-mCherry	Taitool Bioscience	Cat #S0193-9
AAV9-hSyn-DIO-hChR2(H134R)-mCherry	Taitool Bioscience	Cat #S0165-9
AAV2/9-hSyn-DIO-mCherry	Taitool Bioscience	Cat #S0240-9
AAV2/9-hSyn-FLEX-GCaMP6f	Taitool Bioscience	Cat #S0227-9
Chemicals, peptides, and recombinant proteins		
NBQX	Tocris	Cat #0373
D-APV	Tocris	Cat #0106
Biocytin	Sigma	B4261
Clozapine-N-oxide	LKT Laboratories	Cat C4759
Alexa Fluor 647-conjugated cholera-toxin subunit (CTB-647)	Thermofisher	C34778
Alexa Fluor 488-conjugated cholera-toxin subunit (CTB-488)	Thermofisher	C34775
Experimental models: Organisms/strains		
Mouse: VGlut2-IRES-Cre mice	Jackson laboratory	JAX stock #016963
Mouse: ChAT-IRES-Cre mice	Jackson laboratory	JAX stock #006410
GAD67-GFP knock-in mice	Created by Yuchio Yanagawa.	PMID: 14574680
Software and algorithms		
SleepSign	Kissei Comtec	RRID: SCR_018200
Spike2 Software	Cambridge Electronic Design	RRID: SCR_000903
MATLAB R2014b	Mathworks	RRID:SCR_001622
Igor Pro	Wavemetrics	RRID: SCR_000325
FIJI	ImageJ	RRID: SCR_002285
pClamp 10.3	Molecular Devices	RRID: SCR_011323
Olympus FluoView	Olympus	RRID: SCR_014215
GraphPad Prism 8.0	Graphpad	RRID:SCR_002798
Adobe Illustrator	Adobe Systems	RRID: SCR_010279
Other		
microtome	Leica	Cat#CM1950
Vibratome	Leica	Cat#VT1200
pipette puller	Narishige	PC-10

RESOURCE AVAILABILITY

Lead contact

Further information and requests for resources and reagents should be directed to and will be fulfilled by the lead contact, Ya-Dong Li (yadlee@126.com).

Materials availability

This study did not generate new unique reagents.

Data and code availability

- All data reported in this paper will be shared by the lead contact upon request.
- This paper does not report the original codes.
- Any additional information required to reanalyze the data reported in this paper is available from the lead contact upon request.

EXPERIMENTAL MODEL AND STUDY PARTICIPANT DETAILS

Experimental animals

VGlut2-IRES-Cre mice[52] (Slc17a6$^{tm2(cre)Lowl}$, the Jackson Laboratory Stock No: 017535) were provided by Dr. Ji Hu (Shanghai Tech University, Shanghai, China). CHAT-IRES-Cre mice[53] (Jackson Laboratories stock No: 006410) were provided by Zi-Long Qiu (Institute of Neuroscience, Chinese Academy of Sciences). GAD67-GFP knock-in mice[54] were obtained from Yuchio Yanagawa. Only male mice (10–14 weeks old, weighing 22–26 g) were used for experiments. Mice were group-housed (3–5 per cage) under a 12-h (07:00–19:00) light-dark cycle within a colony room at 22°C (humidity ≈60%). Food and water were provided *ad libitum*. All experimental protocols were approved by the Fudan University Animal Care and Use Committee.

METHOD DETAILS

EEG/EMG electrode-implantation surgery

Briefly, mice were anesthetized under 1.5% isoflurane in oxygen at a 0.8-LPM flow rate. Two stainless-steel screws, which served as EEG electrodes, were implanted into the skull above the right cortex (coordinates: anteroposterior [AP]: ±1.0 mm, mediolateral [ML] + 1.5 mm), and two EMG electrodes were implanted in the dorsal neck musculature to monitor muscular activity.[55,56] All EEG electrodes were fixed to the skull via dental cement.

EEG recordings and analysis

EEG recordings and analysis were performed as previously described.[56] Cortical EEG and neck EMG signals were amplified and filtered (Biotex, Kyoto, Japan. EEG, 0.5–30 Hz; EMG, 20–200 Hz). Each frequency band in the EEG was calculated via SleepSign software using the fast Fourier transformation (FFT) method, by dividing the EEG power spectrum into four different frequency bands: delta (0.5–4.0 Hz), theta (4.0–8.0 Hz), alpha (8.0–15 Hz), and beta (16–30 Hz). For FFT analysis, Fourier transformation was used to calculate the power variable (uV^2), and absolute power spectra of the EEG data were computed every 4 s over a 0–25 Hz window with 0.25-Hz resolution. Absolute power spectra were transferred into relative changes (power density) by taking a synchronization value as 100% and analyzing the percent change in each EEG band concerning the synchronization value. For sleep-stage analysis, EEGs and EMGs were automatically classified using 4-s epochs for wakefulness, REM sleep, and NREM sleep according to standard criteria.[57]

Viral injections and fiber implantations

AAV2/9-hSyn-DIO-hM3Dq/hM4Di-mCherry (and control structure: AAV9-hSyn-DIO-mCherry), AAV2/9-hSyn-DIO-ChR2(h134R)-mCherry (and control structure: AAV9-hSyn-DIO-mCherry), and AAV2-hSyn-FLEX-GCaMP6f constructs (titer: 5×10^{12} genomic particles/mL) were used in chemogenetic, optogenetic, and fiber-photometry experiments, respectively. In short, mice were anesthetized with 1.5% isoflurane and placed in a stereotaxic apparatus (RWD, Shenzhen, China), followed by microinjection of 100–200 nL of the construct (AAV2/9-hSyn-DIO-hM3Dq/hM4Di-mCherry or AAV9-hSyn-DIO-mCherry) into the bilateral VP (AP: +0.14 mm, ML: ±1.5 mm, DV: - 4.9 mm) or 200 nL of AAV2-hSyn-DIO-GCaMP6f into the lateral VP. After injections, mice used for *in vivo* optogenetic-stimulation experiments were bilaterally implanted with optical fibers (fiber core, 200 μm; 0.37 numerical aperture (NA), Newdoon, Hangzhou, China) above the VP (AP: +0.14 mm, ML: ±1.5 mm, DV: - 4.6 mm), LH (AP: - 0.94 mm, ML: ±1.1 mm, DV: - 4.0 mm, or LHb (AP: - 1.58 mm, ML: ±0.5 mm, DV:- 2.2 mm).

For fiber photometry, a unilateral fiber was implanted into the lateral VP (AP: +0.14 mm, ML: 1.5 mm, DV: - 4.8 mm).

For anterograde tracing, 100 nL AAV2/9-hSyn-DIO- mCherry was unilaterally injected into lateral VP. For retrograde tracing, CTB-488 and CTB-647 were unilaterally injected into LH and LHb, respectively.

After behavioral tests, mice were sacrificed to verify the proper viral expression.

Fiber photometry

Fiber-photometry experiments were performed as previously described.[4,7,8] In short, to record fluorescent signals, a laser beam was passed through a 488-nm laser (OBIS 488LS; Coherent), reflected off a dichroic mirror (MD498; Thorlabs, USA), focused by an objective lens (Olympus, Japan), and coupled through a fiber-collimation package (F240FC-A, Thorlabs, USA) into a patch cable connected to the ferrule of an upright optical fiber implanted in the mouse via a ceramic sleeve (125-μm O.D.; Newdoon, China). The photometry voltage traces were down-sampled to match the EEG/EMG sampling rate using a Power 1401 digitizer and Spike2 software (CED, Cambridge, UK). Photometry data were exported to MATLAB Mat files from Spike2 for further analysis. We derived the value of the photometry signal (ΔF/F) by calculating (F–F0)/F0, where F0 is the median fluorescent signal. Averaged ΔF/F was calculated during all times of sleep-wake states. For analyzing state transitions, we determined each transition and aligned ΔF/F in a ±50-s window around each point that was calculated. The average peak of the ΔF/F was selected and compared for different sleep stages. For analyzing the activity of glutamatergic VP neurons before and after tail suspension, we recorded the GCaMP6f activity for 5 minutes at home cages before tail suspension as the baseline. Then mice were suspended for 30 minutes with cable. After that, we put the mice back in their home cages and immediately recorded the GCaMP6f activity for the other 5 minutes. GCaMP6f activities over 3*SD were counted as events based on previous studies.[4,23] We set 3*SD as the threshold because it can reflect calcium activity and filter the most insignificant signals. To avoid the bias of counting events, we also analyzed the time of GCaMP6f activities over thresholds/total recording time as time 'above thresholds (%)'. In addition, the mean amplitude of peak ΔF/F of all events was counted as the average peak. For analyzing the activity of VP glutamatergic neurons in elevated plus-maze, calcium activity was analyzed 3 seconds before and after closed-to-open and open-to-closed arm transitions. Six trials for each mouse and five mice in total were included. The average ΔF/F of each mouse in open and closed arms was calculated as mean ΔF/F for comparison.

Optogenetic stimulation *in vivo*

For *in vivo* light stimulation, light-pulse trains were generated via a laser stimulator (SEN-7103, Nihon Kohden, Japan) and output through an isolator (ss-102J, Nihon Kohden, Japan). A rotating optical joint (FRJ_FC-FC, Doric Lenses, Canada) was used to relieve torque. For acute optogenetic stimulation, each epoch was applied 16 s after identifying a stable NREM sleep event by real-time online EEG/EMG analysis. Light-pulse trains (5-ms duration each) were programmed and conducted during the light period when mice were inactive. The cut-off line for stage transitions is 60 s after the laser is on. For chronic photostimulation, programmed light-pulse trains (5-ms pulses at 20/30 Hz, with 10-s on/20-s off for 120 cycles) were used from 09:00 to 10:00. EEG/EMG recordings during the same period on the previous day served as baseline control. The power intensities of blue light at the tip of the optical fiber were measured by a power meter (PM10, Coherent, USA) and calibrated to emit 3–7 mW.[7,8]

For VP^{Vglut2}-LHb circuit stimulation in emotional behaviors tests, blue light-pulse trains (5-ms pulses at 20 Hz) were administrated in both ChR2 and mCherry control mice during tests. For forced swimming tests, blue light-pulse trains (5-ms pulses at 20 Hz, with 300 on/300 off for 1 hour) were used in ChR2 and mCherry control mice, and behavioral tests were carried out immediately after light stimulation to avoid obstruction of cable in mouse swimming.

Behavioral tests

Behavior tests were performed as in previous experiments.[7,23,56]

Elevated plus-maze test (EPM)

The EPM apparatus was made of four plexiglass arms. Each mouse was placed in the center of the intersecting arms, facing an open arm, and was allowed to explore the apparatus for 5 min. An experimenter

blinded to the treatment recorded the time spent in each arm. Behavioral results were determined by measuring the entries and time spent in the open arms.

Open field test (OFT)

The OFT apparatus was a Plexiglas-squared arena (40 × 40 cm) with gray walls (40 cm high) and an open roof. Mice were gently placed in the center of the field, and movement was recorded for 5 min. The locomotion and time spent in the center of the arena (a 20 × 20 cm zone in the center of the apparatus) were measured.

Black-white box test (BWT)

The BWT apparatus (35 cm × 20 cm × 20 cm) consisted of two compartments, with half-painted white and half-painted black. These compartments were separated by a divider with a 3.5 cm × 3.5 cm opening at the floor level. Each mouse was released in the center of the light compartment and allowed to explore the arena for 5 minutes. The number of entries and time spent in the white compartment were recorded.

Tail suspension test (TST)

Mice were suspended by the tail from a metal rod using adhesive tape. The rod was fixed 45 cm above the ground. The test session was recorded for 5 minutes, and the immobility time was determined by an observer blinded to the treatment conditions.

Forced swimming test (FST)

The FST apparatus consisted of an acrylic cylinder (with a diameter of 20 cm and height of 30 cm) filled with water to a depth of 20 cm and maintained at 23 ± 1°C. Each mouse was subjected to a 5 min videotaped swimming trial. Time of immobility was reported as the mouse remained immobile during the test session.

Immunohistochemistry

Immunohistochemistry was performed as described previously. Mice were deeply anesthetized 1.5 h after CNO administration or 0.5 h after light stimulation and were then perfused intracardially with phosphate-buffered saline (PBS) followed by 4% paraformaldehyde (PFA). After brains sank in 30% sucrose solution, coronal slices (30 μm) were cut into four series via a microtome (CM1950, Leica, Germany).

For c-Fos labeling, a primary antibody was incubated at 4°C for 48 h (rabbit anti-c-Fos, 1:10,000; Millipore, USA). Sections were then washed in PBS and incubated for 2 h at room temperature (RT) with donkey anti-rabbit 488 secondary antibody. For biocytin labeling after whole-cell patch-clamp recording slices, tissues containing biocytin-loaded cells were fixed in 4% PFA and were then blocked with 5% donkey serum. Streptavidin conjugated to Alexa 488/647 (1:1000; Invitrogen Molecular Probes, USA) were used. Images were captured using a 40× objective under a confocal microscope (Fluoview 1000, Olympus, Japan).

For VGLUT2 mRNA labeling, *in situ* hybridization was performed using digoxigenin riboprobes on 20 μm frozen sections as described previously.[58] DNA templates for *in situ* hybridization probes were obtained by PCR from either wild-type-embryo or P0-mouse cDNA libraries. The brain sections were mounted onto slides and were surrounded by water-repellent traces. Subsequently, the slides were fixed for 20 min in 4% PFA. Sections were dried and coverslipped with Vectamount (Vector Laboratories).

In vitro electrophysiology

In vitro electrophysiological experiments were performed 3–4 weeks after AAV-ChR2 injections to Vglut2-Cre mice or Vglut2-Cre:GAD67-GFP double-transgenic mice. Mice were anesthetized and perfused transcardially with ice-cold modified aCSF saturated with 95% O2 and 5% CO2 and containing the following (in mM): 215 sucrose, 26 NaHCO3, 10 glucose, 3 MgSO4, 2.5 KCl, 1.25 NaH2PO4, 0.6 Na-pyruvate, 0.4 ascorbic acid, and 0.1 CaCl2. Brains were then rapidly removed, and acute coronal slices (300 μm) containing the VP, LH, or LHb were cut on a vibratome (VT1200, Leica, Germany) in ice-cold modified aCSF. Next, slices were transferred to a holding chamber containing normal recording aCSF (in mM): 125 NaCl, 26 NaHCO3, 25 glucose, 2.5 KCl, 2 CaCl2, 1.25 NaH2PO4, and 1.0 MgSO4. Slices were allowed to recover for 30 min at 32°C. Then, slices were maintained at RT for 30 min before recording. During recording, slices were submerged in a recording chamber superfused with aCSF (2 mL/min) at 30°C–32°C. Slices were visualized using a fixed-stage upright microscope (BX51W1, Olympus, Japan) equipped with a 40× water-immersion

objective and an infrared-sensitive CCD camera. In Vglut2-Cre::GAD67-GFP mice, GAD67-GFP neurons were identified based on their GFP expression. Recordings were performed in regions with bright mCherry fluorescence. Patch pipettes were fabricated from thick-walled borosilicate glass capillaries (1.5-mm outer diameter, 0.86-mm internal diameter, Vital Sense; Scientific Instruments Co., Ltd., China) using a two-step vertical puller (Narishige, PC-10, Japan) and had resistances between 4 MΩ and 6 MΩ. Recording pipettes were filled with an internal solution containing the following (in mM): 105 potassium gluconate, 30 KCl, 10 phosphocreatine, 4 ATP-Mg, 0.3 EGTA, 0.3 GTP-Na, and 10 HEPES (pH 7.3, 285–300 mOsm). In some experiments, 0.1% biocytin (vol/vol, Sigma, USA) was included in the internal solution. Recordings were conducted in the whole-cell configuration using a Multiclamp 700B amplifier (Axon Instruments, USA). Signals were filtered at 2 kHz and digitized at 10 kHz with a DigiData 1440A (Axon Instruments, USA). Data were acquired and analyzed with pClamp10.3 software (Axon Instruments, USA).

Responses were evoked by 5-ms light flashes (473 nm, 10 Hz) delivered from a microscope-mounted blue LED (Lumen Dynamics, Canada) through the objective lens directed onto the slice. In the voltage-clamp mode, cells were held at −65 mV. When needed, 50 μM of D-APV and 20 μM of NBQX were added to block NMDA and AMPA receptors. Cells with Ra changes over 20% were discarded.

QUANTIFICATION AND STATISTICAL ANALYSIS

Data are expressed as the mean ± standard error of the mean (SEM). Statistical significance was assessed using two-tailed paired Student's t-tests to compare total sleep amount and behavioral results between the two groups. One-way, two-way, or repeated-measures analyses of variance (ANOVAs) were used to compare sleep amounts, followed by pairwise comparisons via Turkey post-hoc tests. Two sets of frequencies were analyzed by the chi-square test. A two-tailed p-value <0.05 was considered statistically significant. The results of behavioral tests were compared by unpaired or paired t-tests. All data were analyzed using Prism 8.0 software.